





RESEARCH ARTICLE  
10.1029/2022MS003329

# Simulating the Transport and Rupture of Pollen in the Atmosphere

Tamanna Subba<sup>1,2</sup> , Yingxiao Zhang<sup>1</sup>, and Allison L. Steiner<sup>1</sup> 

<sup>1</sup>Department of Climate and Space Sciences and Engineering, University of Michigan, Ann Arbor, MI, USA, <sup>2</sup>Now at Environmental and Climate Sciences Department, Brookhaven National Laboratory, Upton, NY, USA

**Key Points:**

- The greatest amount of subpollen particles is formed from surface and in-atmosphere humidity-driven primary pollen rupture
- Vertical updrafts lift pollen to the upper troposphere (~12 km) during convective events
- Ruptured pollen can reduce cloud water mixing ratios and slightly increase ice phase hydrometeors aloft

**Correspondence to:**

T. Subba,  
tsubba@umich.edu

**Citation:**

Subba, T., Zhang, Y., & Steiner, A. L. (2023). Simulating the transport and rupture of pollen in the atmosphere. *Journal of Advances in Modeling Earth Systems*, 15, e2022MS003329. <https://doi.org/10.1029/2022MS003329>

Received 3 AUG 2022  
Accepted 3 MAR 2023

**Abstract** Pollen, one type of primary biological aerosol particle (PBAP), is emitted from the terrestrial biosphere and can undergo physical changes in the atmosphere via particle rupture. To examine the fate of pollen and its atmospheric processing, a pollen emission and transport scheme is coupled to the Weather Research and Forecasting Model with Chemistry (WRF-Chem). We simulate the emission of pollen and its impacts on the cloud properties and precipitation in the Southern Great Plains from 12 to 19 April 2013, a period with both high pollen emissions and convective activity. We conduct a suite of ensemble runs that simulate primary pollen and three different pollen rupture mechanisms that generate subpollen particles, including (a) high humidity-induced surface rupture, (b) high humidity-induced in-atmosphere plus surface rupture, and (c) lightning-induced rupture, where in-cloud and cloud-to-ground lightning strikes trigger pollen rupture events. When relative humidity is high (>80%), coarse primary pollen (~1 μg m<sup>-3</sup>) is converted into fine subpollen particles (~1.2e<sup>-4</sup> μg m<sup>-3</sup>), which produces 80% more subpollen particles than lightning-induced rupture. The in-atmosphere humidity-driven rupture predominantly produces subpollen particles, which is further enhanced during a frontal thunderstorm. During strong convection, vertical updrafts lift primary pollen and subpollen particles (~0.5e<sup>-4</sup> μg m<sup>-3</sup>) to the upper troposphere (~12 km) and laterally transports the ruptured pollen in the anvil top outflow. In regions of high pollen and strong convection, ruptured pollen can influence warm cloud formation by decreasing low cloud (<4 km) cloud water mixing ratios and increasing ice phase hydrometeors aloft (>10 km).

**Plain Language Summary** Biological aerosols like pollen are released from the terrestrial biosphere into the atmosphere and affect atmospheric processes, hydrology, and climate. For example, large primary pollen ruptures in different atmospheric conditions to produce multiple small-sized pollen fragments. Moreover, these ruptured particles can trigger thunderstorm asthma. In this study, a Weather Research and Forecasting Model with Chemistry was used to evaluate the fate of pollen in the atmosphere. Model simulations indicate that the three pollen rupture mechanisms, including high humidity-induced surface rupture, in-atmosphere plus surface rupture, and lightning-induced rupture, influence the overall pollen load over the Southern Great Plains during convective days with high pollen emissions. The SPP are produced in the highest concentrations in the atmosphere and on the surface due to the high relative humidity-induced-rupture. Even though in-cloud and cloud-to-ground lightning strikes trigger pollen rupture events, they cannot produce as much as humidity-induced ruptures. The ruptured pollen is transported to higher altitudes by vertical updrafts, horizontally through the outflows from the top of the clouds, and finally to the surface by the downdraft. In regions of high pollen and strong convection, ruptured particles can further alter the hydrometeors and influence cloud formation.

## 1. Introduction

Atmospheric aerosols influence Earth's climate through their interactions with radiation and clouds, thereby influencing the overall hydrological cycle (Bellouin et al., 2020; Christensen et al., 2020; IPCC, 2021). Primary biological aerosol particle|Primary biological aerosol particles (PBAP) are particles directly emitted from the Earth's surface and include bacteria, cellular matter, decayed organic matter, fungi, plant fragments, pollen, and spores (Despres et al., 2012). PBAP, like other aerosol particles, can impact atmospheric processes (Despres et al., 2012; Fröhlich-Nowoisky et al., 2009; Jaenicke, 2005; Lawler et al., 2020; Sofiev et al., 2006) by influencing clouds and precipitation as cloud condensation nuclei (CCN) (Ariya et al., 2009; Sun & Ariya, 2006) and ice nucleating particles (INP) (Burkart et al., 2021; Diehl et al., 2001; Dreischmeier et al., 2017; Gute & Abbatt, 2018; Murray et al., 2012; Pummer et al., 2012), which affect the overall climate and hydrological cycle

© 2023 The Authors. Journal of Advances in Modeling Earth Systems published by Wiley Periodicals LLC on behalf of American Geophysical Union. This is an open access article under the terms of the [Creative Commons Attribution License](https://creativecommons.org/licenses/by/4.0/), which permits use, distribution and reproduction in any medium, provided the original work is properly cited.

(e.g., Andreae & Rosenfeld, 2008; Joung et al., 2017; Pöschl et al., 2010; Wozniak et al., 2018; Y. Zhang & Steiner, 2022; R. Zhang et al., 2014; Y. Zhang et al., 2014). Primary pollen can further act as a giant CCN, due to their size and hygroscopicity, which may influence cloud formation processes (Posselt & Lohmann, 2008; Tang et al., 2019; Yin et al., 2000).

Anemophilous plants (i.e., those with wind-driven pollination strategies) emit the greatest number of pollen grains into the atmosphere (Jones & Harrison, 2004; Lewis et al., 1983; Straka, 1975), and the spatial distribution of pollen emissions depends on the vegetation species or plant functional type. Emissions have a strong variability depending on their flowering time (Wozniak & Steiner, 2017; Y. Zhang & Steiner, 2022), their physical (shape, density, and viability) characteristics (Despres et al., 2012; Helbig et al., 2004; Veriankaitè et al., 2010), and meteorological (e.g., temperature, wind, humidity, precipitation, and friction velocity) and climatological (e.g., temperature, soil moisture, and CO<sub>2</sub>) conditions. Additionally, atmospheric pollen concentrations can be altered via anthropogenic activities such as land-use patterns, urbanization, and extreme weather conditions like thunderstorms and lightning (Hughes et al., 2020; Sofiev et al., 2006; R. Zhang et al., 2014; Y. Zhang et al., 2014; Ziska et al., 2011).

Observations of pollen are limited surface observations, which are sparsely distributed. Additionally, the relatively large size of pollen grains has led to their exclusion in many observational aerosol networks. Most atmospheric aerosol models have focused instead on the simulation of PM<sub>2.5</sub>, which has known health effects, can influence climate, and has a broader suite of analytical tools for observations. Pollen transport within and above the atmospheric boundary layer is poorly constrained, with few observations and modeling studies investigating the vertical and spatial distributions. Surface temperature and humidity can affect pollen transport, with cooler and moister conditions limiting emissions (Jones & Harrison, 2004). In previous studies, back trajectory analysis has identified long-range transport, which is possible via mechanical and thermally induced turbulent eddies that lift emissions into the atmospheric boundary layer (Kuparinen, Markkanen, et al., 2007; Mahura et al., 2007) and is vital to plant ecology and evolution (Kuparinen et al., 2009; Nathan et al., 2011; Tackenberg, 2003). However, a complete analysis of pollen transport in the atmosphere has yet to be conducted.

Primary pollen grains can be processed and altered within the atmosphere. Under high humidity, large-sized primary pollen grains are known to rupture due to osmotic shock, forming small fragments (subpollen particles, SPP) ranging from 30 nm to 5 μm (Emmerson et al., 2021; Grote et al., 2001, 2003; Miguel et al., 2006; A. L. Steiner et al., 2015; Stone et al., 2021; Taylor & Jonsson, 2004; Taylor et al., 2004). While rainfall can reduce pollen counts by wet deposition (Hughes et al., 2020), moist conditions can also cause pollen rupture (Rathnayake et al., 2017; Wozniak et al., 2018). Field observations suggest that pollen fragments peak during rainfall and remain in the atmosphere for several hours afterward (Rathnayake et al., 2017). Hughes et al. (2020) is the first field study to measure potential SPP before, during, and after thunderstorm events and found a significant increase in SPP with diameters of 0.25–1.0 μm during precipitation in Iowa City, Iowa during the spring tree pollen season (April–May 2019). They used single-particle fluorescence spectroscopy with offline measurements of chemical tracers and found that pollen fragments were most abundant during convective thunderstorms with strong downdrafts and lightning strikes.

Pollen is a common allergen (Andrew et al., 2017; D'Amato et al., 2016), so understanding its emission, transport, and fate in the atmosphere is increasingly important. The significance of the pollen-asthma relationship varies between studies depending on the pollen type and the surrounding meteorological conditions. Over the last few decades, numerous epidemiological studies have examined the relationship between exposure to different pollen types and asthma-related Emergency Department visits in various locations in the United States (e.g., Anenberg et al., 2017; Babin et al., 2007; Darrow et al., 2012; Neumann et al., 2019; Pollock et al., 2017), Canada (Dales et al., 2004, 2008), Australia (Andrew et al., 2017; Emmerson et al., 2021), Europe (Lake et al., 2016), and Asia (Yair et al., 2019).

Several studies have reported increased asthma morbidity during thunderstorms leading to a phenomenon known as “thunderstorm asthma” (Bannister et al., 2020; Beggs, 2017; D'Amato et al., 2019; Emmerson et al., 2021). The thunderstorm asthma hypothesis suggests that pollen grains are processed within a thunderstorm and ruptured, either due to high humidity-induced osmotic shock (Beggs, 2017) or lightning-induced osmotic shock (Emmerson et al., 2021; Hughes et al., 2020; Newson et al., 1998), causing the larger primary pollen grains to rupture into smaller fragments that are easily dispersed by strong thunderstorm winds (Taylor & Jonsson, 2004). Compared to primary pollen, the smaller-sized SPP can persist in the atmosphere longer and are easily inhalable

as cytoplasmic allergens. Around 20 epidemic thunderstorm asthma events have been reported (Kevat, 2020). Several studies combining allergy, pulmonology, meteorology, and climatology perspectives have established the relationship between thunderstorm asthma and asthma morbidity (Dales et al., 2004; D'Amato et al., 2016; Emmerson et al., 2021; Hughes et al., 2020; Kevat, 2020; Yair et al., 2019; Ziska et al., 2011). Yair et al. (2019) reported the first case of thunderstorm asthma in Israel on 25 October 2015, where a storm with intensive lightning activity, hail, downbursts, and heavy rain coincided with the peak of *Ambrosia* pollen. Melbourne, Australia experienced the world's largest thunderstorm asthma event on 21 November 2016 coinciding with the peak grass pollen season, in a brief period resulting in thousands of casualties (672% of the average overnight casualties) and several deaths (Andrew et al., 2017; Bannister et al., 2020; Emmerson et al., 2021; Thien et al., 2018). This event occurred during a dry thunderstorm period associated with a gust front sweeping eastwards through the city. These two studies are representative of two different types of thunderstorm events (one with precipitation and one without) that have triggered severe thunderstorm asthma episodes across the globe.

High resolution atmospheric modeling can provide insight into pollen's atmospheric fate and its impact on cloud processes and human health. R. Zhang et al. (2014) and Y. Zhang et al. (2014) developed a regional-scale pollen emission and transport modeling framework over Southern California that treated pollen as a non-reactive tracer within the coupled Weather Research and Forecasting - Community Multiscale Air Quality (WRF/CMAQ) model. Pollen rupture mechanisms have recently been included in models, such as Wozniak et al. (2018) who used a regional climate model to simulate pollen rupture during spring pollen season in the United States and estimated its influence on precipitation. Emmerson et al. (2021) evaluated the Melbourne thunderstorm asthma event with several possible pollen rupture mechanisms, including mechanical friction, lightning strikes, and relative humidity, concluding that the lightning rupture mechanism was the most efficient SPP generator in this case.

In this study, we model the fate of pollen and the possibilities for their rupture over the Southern Great Plains (SGP) in the United States during the simultaneous occurrence of high pollen emissions and thunderstorms with lightning activity in April 2013. We have developed a pollen module that adds primary biological particles (primary pollen and subpollen (POLs) particles) as a new aerosol species within the WRF-Chem model (Grell et al., 2005) by incorporating pollen into the MADE/Secondary Organic Aerosol Model (SORGAM) aerosol framework (Schell et al., 2001). The Pollen Emissions for Climate Models version 2.0 (PECMv2.0) (Y. Zhang & Steiner, 2022) provides the hourly pollen emission flux during the phenological cycle, which is further coupled with online meteorology. We include different pollen rupture mechanisms (including both moisture and lightning-driven rupture) and examine the effect of these particles on cloud formation and hydrometeor evolution. Hypothesizing that the seasonal timing and transport of pollen and their rupture may influence mesoscale atmospheric phenomena, our objectives are to (a) examine the fate of pollen and the possibility of their rupture and (b) understand the relative contribution of meteorological conditions to the variability in modeled pollen and vice versa, and (c) evaluate the effect of these particles on warm cloud formation and hydrometeor evolution during a thunderstorm with the lightning event. As a result, this work provides essential input to studies related to the climatic impact of PBAPs, climate-related changes in airborne pollen, and human health.

## 2. Methodology

### 2.1. Pollen Modeling Framework

We incorporate pollen within the WRF-Chem modeling (Grell et al., 2005) framework to simulate its emissions, transport, and fate in the atmosphere. The coupled framework of WRF-Chem includes the presence of pollen to feedback on cloud and radiative processes, allowing us to investigate the impact of pollen on cloud formation processes. Pollen emissions are incorporated into the WRF-Chem model (Figure 1) and coupled with a new module for pollen within the Modal Aerosol Dynamics Model for Europe (MADE) (Ackermann et al., 1998) aerosol model that implements the SORGAM of Schell et al. (2001) (MADE/SORGAM). MADE uses the modal approach to represent the aerosol size distribution with three log-normal modes, that is, Aitken mode ( $<0.1 \mu\text{m}$  diameter, with median diameter of  $0.01 \mu\text{m}$  and standard deviation of 1.6; Ackermann et al., 1998), the accumulation mode ( $0.1\text{--}2.0 \mu\text{m}$  diameter, with median diameter of  $0.07 \mu\text{m}$  and standard deviation of 2.0; Ackermann et al., 1998) and the coarse mode ( $>2 \mu\text{m}$  diameter).

We embed the pollen module alongside the SORGAM framework and other aerosol emissions, including anthropogenic emissions, biomass-burning, sea salt, and dust. We add two new aerosol indices via this module, including

Schematic representation of POLLEN-WRF/CHEM modeling framework

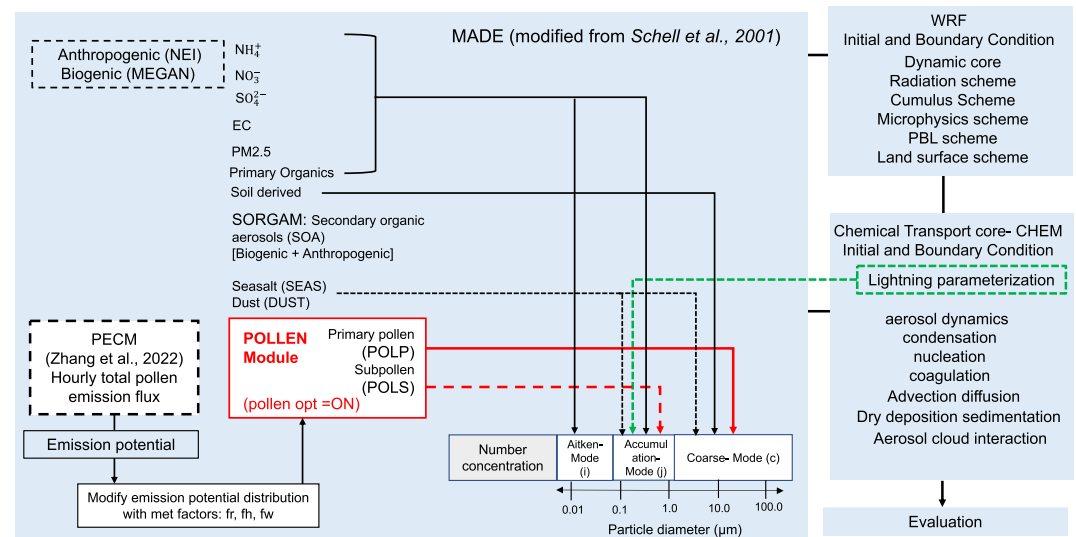


**Figure 1.** Schematic representation of the pollen module within the MADE-SORAGAM aerosol chemistry module in the WRF-Chem modeling framework (after Schell et al. (2001)). The pollen module is embedded alongside the Secondary Organic Aerosol Model framework together with other aerosol emissions, including anthropogenic emissions, biomass burning, sea salt, and dust. Here, we add two new aerosol indices via this module, including (1) POLP (primary pollen) to represent the coarse biological aerosol concentration and (2) pollen and subpollen (POLS) (subpollen particles) in the accumulation mode biological aerosol concentration. For emissions, we use the Pollen Emissions for Climate Models version 2.0 (PECEMv2.0; Y. Zhang & Steiner, 2022), which provides the total emission potential to simulate pollen counts over the United States. Along with the high humidity condition, the lightning parameterization (Barth et al., 2014) is called to rupture POLP to POLS via lightning.

(a) POLP (primary pollen) to represent the coarse biological aerosol concentration and (b) POLS (subpollen particles) in the accumulation mode biological aerosol concentration. Pollen thus represents an additional aerosol species of biological origin that are added to two different aerosol modes and subject to all major atmospheric processes, including emissions, transport, gas-aqueous-phase chemistry, influence on radiative properties and cloud formation, and wet and dry deposition.

For emissions, we use the Pollen Emissions for Climate Models version 2.0 (PECEMv2.0; Y. Zhang & Steiner, 2022), which provides the total emission potential to simulate pollen counts over the United States. The climate-flexible PECEMv2.0 model uses modern surface pollen count data and empirical relationships between prior-year annual average temperature to develop pollen season start dates and end dates. In addition, the model produces emission potentials for the most prevalent wind-pollinating taxa in the United States, including nine genera of deciduous broadleaf trees (DBF, including *Acer* or maple, *Alnus* or alder, *Betula* or birch, *Fraxinus* or ash, *Morus* or mulberry, *Platanus* or plane, *Populus* or poplar, *Quercus* or oak, *Ulmus* or elm), two families of evergreen needleleaf trees (ENF, including *Cupressaceae* or cypress, *Pinaceae* or pine), grasses (*Poaceae*; C3, C4), and one type of weed (*Ambrosia* or ragweed). To reduce the number of additional tracers, we group all pollen types and simulate total pollen only.

The pollen module couples pollen emission fluxes with the online meteorology and converts primary pollen into subpollen particles via different rupture mechanisms depending on the existing meteorological conditions. The overall effective mean grain diameter of POLP is  $>10 \mu\text{m}$ , based on Wozniak et al. (2018), that used the University of Cambridge Pollen Image Library to classify the diameters of the DBF vegetation ( $28 \mu\text{m}$ ), ENF vegetation ( $40 \mu\text{m}$ ), grasses ( $35 \mu\text{m}$ ), and ragweed ( $20 \mu\text{m}$ ) with all assuming a similar mass density of  $1,200 \text{ kg m}^{-3}$  based on measurements (Davis & Brubaker, 1973). For the POLS, the mean grain diameter is assumed to be  $\sim 0.15 \mu\text{m}$  (based on the most hygroscopic of the POLS size bins; A. L. Steiner et al., 2015) with a mass density of  $1,450 \text{ kg m}^{-3}$ , based on the mean of the mass densities typical of protein ( $1,350 \text{ kg m}^{-3}$ ; average from Table 1 in Fischer et al. (2004)) and starch ( $1,500 \text{ kg m}^{-3}$  for air-equilibrated starch; Dengate et al., 1978; Marousis & Saravacos, 1990) molecules that likely comprise subpollen particles (A. L. Steiner et al., 2015). Because PBAP is almost entirely organic (Despres et al., 2012), the physical and optical properties of POLP and POLS are treated

like organic carbon in MADE-SORGAM with a molecular weight of 80.44 g/mol and 44.44 g/mol for POLP and POLS respectively, and hygroscopicity as 0.25 and 0.14 for POLP and POLS, respectively.

The pollen module is divided into two sections. First, the daily total pollen emission potential ( $E_{\text{pot}}$ , in grains  $\text{m}^{-2} \text{s}^{-1}$ ) from PECMV2.0 is called for each grid cell.  $E_{\text{pot}}$  is modified by the online meteorology (Equation 1), including grid cell wind (Equation 2), precipitation (Equation 3), and relative humidity (Equation 4) using parameterizations developed in Sofiev et al. (2013) to calculate the total pollen emissions ( $E_{\text{pol}}$ ) (Equation 1):

$$E_{\text{pol}} = E_{\text{pot}} \times f_w \times f_r \times f_h \quad (1)$$

The factors  $f_w$ ,  $f_r$ , and  $f_h$  represent wind, rain, and relative humidity factors that influence total pollen emission potential. The following are defined as:

$$f_w = 1.5 - e^{-\frac{|u_{10}|}{5}} \quad (2)$$

$$f_r = \begin{cases} 1, & \text{rain} < \text{rain}_{\text{low}} \\ \frac{\text{rain}_{\text{high}} - \text{rain}}{\text{rain}_{\text{high}} - \text{rain}_{\text{low}}}, & \text{rain}_{\text{low}} < \text{rain} < \text{rain}_{\text{high}} \\ 0, & \text{rain} > \text{rain}_{\text{high}} \end{cases} \quad (3)$$

$$f_h = \begin{cases} 1, & \text{relhum} < \text{relhum}_{\text{low}} \\ \frac{\text{relhum}_{\text{high}} - \text{relhum}}{\text{relhum}_{\text{high}} - \text{relhum}_{\text{low}}}, & \text{relhum}_{\text{low}} < \text{relhum} < \text{relhum}_{\text{high}} \\ 0, & \text{relhum} > \text{relhum}_{\text{high}} \end{cases} \quad (4)$$

The meteorological parameters in Equations 2–4 are from online WRF-Chem grid-cell resolution variables, including “ $u_{10}$ ” as the 10-m horizontal wind speed, “rain” as surface precipitation rate ( $\text{mm hr}^{-1}$ ), and “relhum” as 10-m relative humidity (%) with low and high thresholds of  $\text{rain}_{\text{high}} = 0.5 \text{ mm hr}^{-1}$ ,  $\text{rain}_{\text{low}} = 0 \text{ mm hr}^{-1}$ ,  $\text{relhum}_{\text{high}} = 80\%$ , and  $\text{relhum}_{\text{low}} = 50\%$ . These thresholds obtained by Wozniak et al. (2018) are based on Sofiev et al. (2013) and Linkosalo et al. (2010).

## 2.2. Pollen Rupture Mechanisms

Due to the uncertainties in mechanisms of pollen rupture, we added three rupture mechanisms in WRF-Chem to generate POLS, including (a) high humidity or precipitation-induced surface rupture and (b) high humidity or precipitation-induced surface plus in-atmosphere rupture, and (c) lightning-induced rupture. These three mechanisms are tested and evaluated in Sections 3.2 and 3.3 of the manuscript.

### 2.2.1. Humidity Induced Surface Rupturing

At the surface, we assume that pollen on cones or anthers of flowers may rupture when exposed to moisture during precipitation or when surface humidity is high. This hypothesis is based on laboratory studies of birch and grass pollen (Taylor et al., 2002, 2004). If surface conditions promote rupture, ruptured particles (designated in the model as POLS) are released from the primary pollen grains (defined in the model as POLP) into the ambient atmosphere. For a given atmospheric model grid volume at the surface ( $i = 1$ ), when the relative humidity is equal to or greater than 80%, the rupture flag is turned on ( $\text{rupture} = 1$ ) to allow the POLP to rupture and produce POLS:

$$\text{POLS}_{i=1} = \text{POLP}_{i=1} \times F_{\text{rupt}} \times n_{\text{spg}} \times \frac{m_{\text{POLS}}}{m_{\text{POLP}}} \quad (5a)$$

Where the fraction of POLP ruptured and converted to POLS ( $F_{\text{rupt}}$ ) is assumed to be 0.7, following Taylor et al. (2002) and Wozniak et al. (2018). Here  $m_{\text{POLP}}$  and  $m_{\text{POLS}}$  are mass of POLP and POLS. Following Suphioglu et al. (1992) and Stone et al. (2021), the conversion factor from primary pollen to subpollen ( $n_{\text{spg}}$ ) is estimated to be 1,000 subpollen particles (i.e., 1 POLP grain produces  $\sim 1,000$  POLS grains).

Further, the fraction of the POLP converted to POLS is subtracted from the total POLP:

$$\text{POLP}_{i=1} = \text{POLP}_{i=1} \times (1 - F_{\text{rupt}}) \quad (5b)$$



If the relative humidity is <80%, the rupture flag is turned off ( $F_{rupt} = 0$ ), and no POLS is produced.

### 2.2.2. Humidity Induced Surface Plus In-Atmosphere Rupturing

For the second rupture mechanism, the above process is repeated for the entire atmospheric column ( $i = 2$  to  $N$ ) at each atmospheric layer including the surface ( $i = 1$ ):

$$POLS_{i=1,N} = POLP_{i=1,N} \times F_{rupt} \times n_{spg} \times \frac{m_{POLS}}{m_{POLP}} \quad (6a)$$

$$POLP_{i=1,N} = POLP_{i=1,N} \times (1 - F_{rupt}). \quad (6b)$$

The same relative humidity threshold is used as at the surface (>80%) to determine if atmospheric rupture occurs.

### 2.2.3. Lightning Induced Rupturing

The third pollen rupture mechanism is that induced by lightning. Lightning is simulated online in WRF-Chem using the parameterization of Barth et al. (2014), which includes a two-dimensional (e.g., lat/lon) in-cloud (IC) and cloud-to-ground (CG) lightning flash rates within each model grid cell. The gridded flash rate (lightning strikes per second) triggers pollen rupture events. With every lightning strike, we assume that ~10% of the POLP converts into POLS and using the same rupture production rates as observed in humidity studies (1 POLP produces 1,000 POLS; Stone et al., 2021; Suphioglu et al., 1992). There are two large uncertainties in this rupture mechanism: (a) it is unknown if lightning-induced rupture would provide the same number of POLS as humidity-induced rupture, and (b) the efficiency of lightning rupture is also unconstrained. In this study, we test the rupture fraction ( $F_{rupt}$ ) with a value of 0.10, as we do not expect that a lightning flash would rupture all the pollen within a model grid cell:

$$POLS_{i_{cldfra>0.3}=N_{cb},N_{ct}} = POLP_{i_{cldfra>0.3}=N_{cb},N_{ct}} \times F_{rupt} \times n_{spg} \times IC\_lightning \text{ flash rate (in-cloud)} \times \frac{m_{POLS}}{m_{POLP}} \quad (7a)$$

where  $i$  indicates the number of in-cloud layers in the atmosphere, and

$$POLS_{i_{cldfra<0.3}=1,N_{cb}} = POLP_{i_{cldfra<0.3}=1,N_{cb}} \times F_{rupt} \times n_{spg} \times CG\_lightning \text{ flash rate (cloud-to-ground)} \times \frac{m_{POLS}}{m_{POLP}} \quad (7b)$$

where the IC flash rates are applied within the cloud layer when the cloud fraction “cldfra” >0.3, and is applied from the cloud base layer ( $N_{cb}$ ) to the cloud top layer ( $N_{ct}$ ). CG flash rates are applied to low cloud layers (cloud fraction <0.3) in the layers between the cloud base layer ( $N_{cb}$ ) to the model ground layers ( $i = 1$ ).

## 2.3. Model Domain and Configuration

Figure 2 shows the WRF-Chem model domain centered on the SGP of the United States (US) bounded by 30–42°N and 90–105°W. The SGP is the developing ground for severe weather events in the Central US, and the SGP experiences frequent thunderstorms that are amongst the strongest globally (Maupin et al., 2021). The SGP region is influenced by the Great Plains Low-Level Jet (LLJ) and its associated moisture flux during the late spring and summer over the central and eastern United States, which is connected with severe weather systems in the central US (Arritt et al., 1997; Maddox, 1983; Mo & Berbery, 2004). Aerosols are known to play a role in cloud development and can modify the systems that develop in the SGP, and moderate aerosol loading persists over the region (Fan et al., 2013; Parworth et al., 2015; Penner et al., 2004). The comprehensive, long-term measurements from the DOE SGP ARM site by Parworth et al. (2015) indicate that submicron bulk aerosols exhibit high interannual variability, with their highest mass concentrations in the summer (~20  $\mu\text{g m}^{-3}$ ) and the lowest in the autumn (~5  $\mu\text{g m}^{-3}$ ). Composition is dominated by total organics (~55% of the aerosol mass), followed by nitrate (16%), sulfate (~20%), and ammonium (~9%). Though the SGP site lacks direct PBAP measurements except for short field campaigns (Knopf et al., 2021), Subba et al. (2021) utilized ground and satellite observations of bulk aerosols and meteorological measurements to detect possible PBAP primary emissions and rupture events from pollen and fungal spores and found that they could occur up to about 30 days  $\text{yr}^{-1}$ . For pollen, ~12 days  $\text{yr}^{-1}$  were identified as primary pollen event days, with ~4 days  $\text{yr}^{-1}$  showing rupture events during and after ~10 hr of rainfall. To understand the role of the severe thunderstorm and lightning on the pollen emission

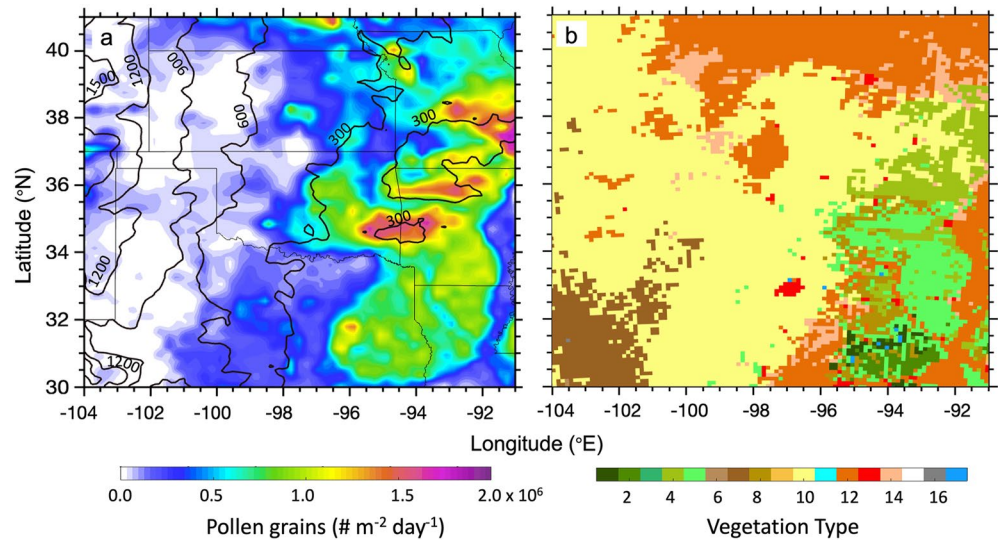


**Figure 2.** WRF-Chem simulation domain with averaged (12–19 April 2013) (a) daily pollen flux from PECMv2.0 model ( $\text{grains m}^{-2} \text{d}^{-1}$ ; color contours), orography (m MSL, brown contours), and black contours show the state boundaries; (b) WRF Vegetation classes comprising of (1) Evergreen Needleleaf Forest, (2) Evergreen Broadleaf Forest, (3) Deciduous Needleleaf Forest, (4) Deciduous Broadleaf Forest, (5) Mixed Forest, (6) Closed Shrubland, (7) Open Shrubland, (8) Woody Savanna, (9) Savanna, (10) Grassland, (11) Permanent Wetlands, (12) Cropland, (13) Urban and Build-up, (14) Cropland/Natural Mosaic, (15) Snow and Ice, (16) Barren or Sparsely Vegetated, and (17) Water.

and their role in hydrometeor evolution, we simulate from 12 to 19 April 2013, when relatively high pollen emissions are present (Subba et al., 2021) in conjunction with severe storms (<https://www.spc.noaa.gov>).

The total pollen emission potential ( $E_{\text{pot}}$ ) is the greatest (up to  $\sim 2 \times 10^6 \text{ grains m}^{-2} \text{d}^{-1}$ ) over forested regions (including Evergreen, Deciduous Needleleaf, Deciduous, and Mixed Forest vegetation types), with lower emissions ( $\sim 0.5 \times 10^6 \text{ grains m}^{-2} \text{d}^{-1}$ ) over grassland and cropland areas (Figure 2b). We conduct three ensemble simulations for each sensitivity experiment discussed in Section 3.4 at a 12 km horizontal resolution with 45 vertical layers. The limitations of the coarser horizontal resolution ( $12 \times 12 \text{ km}$ ) in these simulations may include some loss of evidence of pollen transport and their consequent impacts. Additionally, this may further enhance uncertainty in the role of aerosols in cloud formation processes as the model representation of clouds, lightning, and overall atmospheric controls themselves may be limited. These limitations are discussed in detail in their respective sections.

The overall model configuration is described in Table 1. We allow POLS to act as a CCN and influence warm cloud formation processes. Although pollen has been shown to act as INP in previous studies (Diehl et al., 2001), we have not modified the standard ice nucleation parameterization in WRF-Chem to be aerosol-aware, and the current parameterization simulates ice concentrations as a function of temperature only. For cloud microphysics, we use Morrison microphysics having five hydrometeors (cloud, rain, snow, ice, and graupel) (Morrison et al., 2005). In the current Morrison scheme, the secondary ice formation is turned on via Rime-Splintering (Hallett & Mossop, 1974), and the primary ice nucleation is simulated based on immersion, deposition, contact, and homogeneous freezing (Bigg, 1953; Cooper, 1986; Meyers et al., 1992). Future work will include the development of an aerosol-aware parameterization that can allow for pollen to act as an INP.

#### 2.4. Model Sensitivity Tests

Because the physical processes surrounding rupture are uncertain (Section 2.2), we test the different rupture mechanisms in WRF-Chem with a series of sensitivity tests (Table 2) using the configuration outlined in Table 1. All simulations include primary and secondary aerosols from anthropogenic and biogenic emissions, with sensitivity tests modifying only the treatment of primary and subpollen processes. The first experiment (EXP1) includes no pollen. The second experiment (EXP2) only has primary pollen (POLP), with no rupture (POLS). The third experiment (EXP3) has both primary POLS with precipitation or humidity-induced rupturing only at

**Table 1**  
*Model Configuration*

Simulation period	12–19 April 2013
Domain	30 to 41°N and –104 to –90°E Southern Great Plains United States
Horizontal resolution (dx)	12 × 12 km
Vertical resolution	45 layers from 1,000 to 50 mb
Meteorological IC and BC	North America mesoscale (NAM) forecast output at T221 (32-km) resolution, 28 vertical levels
Shortwave radiation	Goddard shortwave radiation scheme (Chou et al., 1998)
Longwave radiation	The rapid radiative transfer model (RRTM) (Mlawer et al., 1997)
Land surface	Community National Center for Environmental Prediction (NCEP), Oregon State University, Air Force, and Hydrologic Research Lab-NWS Land Surface Model (NOAH) (Chen & Dudhia, 2001)
Surface Layer	Monin-Obukhov (Monin & Obukhov, 1954; Janjic, 2002)
PBL	Yonsei University Scheme (YSU) (Hong et al., 2006)
Cumulus	The Grell scheme (Grell & Devenyi, 2002)
Microphysics	Morrison 2-moment scheme (Morrison et al., 2005)
Chemical mechanism	RADM2 Regional Acid Deposition Model version 2 chemical mechanism (Stockwell et al., 1990)
Chemical initial and boundary conditions	MOZBC from the Model for Ozone and Related chemical Tracers (MOZART) model (Emmons et al., 2010)
Anthropogenic emissions	National Emissions Inventory (NEI)US EPA ( <a href="http://www.epa.gov">www.epa.gov</a> )
Biogenic emissions	The Model of Emissions of Gases and Aerosols from Nature version MEGAN v2.1 biogenic emissions (Guenther et al., 2012)
Pollen emissions	The Pollen Emissions for Climate Models version 2.0 (PECMv2.0; Y. Zhang & Steiner, 2022)

the surface (e.g., within the first model level) (Section 2.2.1). The fourth experiment (EXP4) includes POLP and POLS, with rupture occurring at the surface and in the atmosphere based on the relative humidity constraints (Section 2.2.2). Finally, the fifth experiment (EXP5) includes POLP and POLS induced by lightning-induced rupture (Section 2.2.3). Each of these experiments is carried on as an ensemble of three times of model simulations.

### 3. Results

#### 3.1. Simulation Evaluation

For the 12–19 April 2013 simulation period, we evaluate the simulation with ground-based observations of aerosols and precipitation. We utilize  $PM_{10}$  and  $PM_{2.5}$  from seven Interagency Monitoring of Protected Visual Environments (IMPROVE) sites (Malm et al., 1994) and four Environmental Protection Agency (EPA) ([www.epa.gov](http://www.epa.gov)) sites in the region (Figure 3). IMPROVE  $PM_{10}$  and  $PM_{2.5}$  data collected every third day (i.e., 13, 16, and 19 April 2013) are compared with simulated aerosols. In addition, simulated rainfall is compared with Tropical Rainfall Measuring Mission measurements. For this evaluation, we utilized EXP4 since it best represents the predominant contribution of POLS.

**Table 2**  
*Description of WRF-Chem Pollen Sensitivity Tests*

Experiment no.	Pollen production
EXP1	No pollen
EXP2	Primary pollen (POLP)
EXP3	Primary pollen (POLP) and subpollen (POLS) produced due to high humidity at the surface
EXP4	Primary pollen (POLP) and subpollen (POLS) produced due to high humidity at the surface and in the atmosphere
EXP5	Primary pollen (POLP) and subpollen (POLS) are produced due to lightning inside the cloud (via in-cloud lightning) and from cloud to ground (via cloud-to-ground lightning)



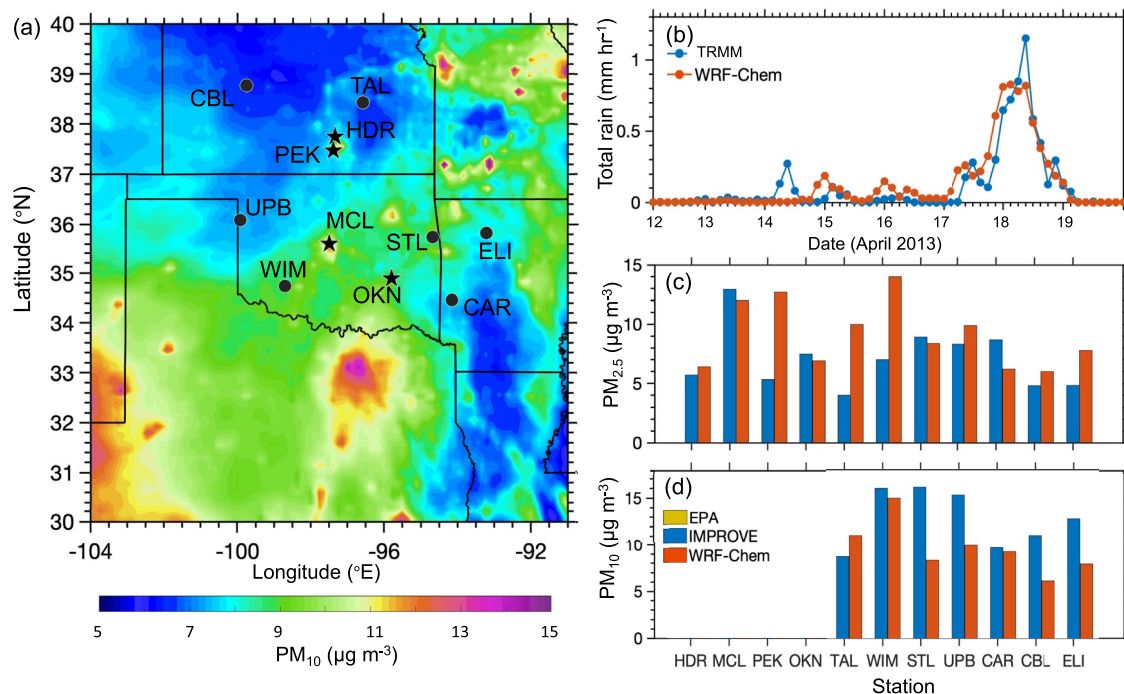


**Figure 3.** For the model simulation period 12–19 April 2013, the (a) spatial distribution of modeled  $PM_{10}$  concentration; (b) observed (blue), and modeled (red) daily rainfall averaged over the spatial domain shown in (a); (c) Interagency Monitoring of Protected Visual Environments (IMPROVE) (blue), and Environmental Protection Agency (EPA) (cyan) observed  $PM_{2.5}$  as compared with modeled  $PM_{2.5}$  (red) averaged over all sampling periods; and (d) IMPROVE (blue) observed  $PM_{10}$  compared with modeled  $PM_{10}$  (red) averaged over all sampling periods in the simulation period. Stars in (a) represent the EPA sites (HDR, Hydraulic; MCL, McAlester; PEK, Peck; OKN, Okc North), and the filled circles represent the IMPROVE sites (CBL, Cedar Bluff; TAL, Tall Grass; WIM, Wichita Mountain; STL, Stillwell; UPB, Upper Buffalo; CAR, Caney Creek; ELI, Ellis).

Previous studies have shown that the SGP region experiences moderate aerosol concentrations ( $\sim 5\text{--}15\text{ mg m}^{-3}$ ) associated with the local anthropogenic emissions such as vehicular, industrial, agricultural, and biomass burning (Kawecki & Steiner, 2018; Parworth et al., 2015), and local natural emissions such as soil dust, PBAPs (Subba et al., 2021), natural biomass burning (Donovan et al., 2017; Melvin, 2018; NIFC, 2019; J. L. Steiner et al., 2020) and aerosols from long-range transport (Parworth et al., 2015; Subba et al., 2021).

EXP4 simulated domain-average rainfall agrees well with observations (correlation of 0.91) with an overestimation of  $\sim 13\%$  (0.02 mm/day). However, there is a slight discrepancy with the rainfall timing. The model simulates an earlier onset of rainfall on 14 April and a delay on 16 April as compared to the measurements. Precipitation timing and the early onset in the model may affect the removal and addition of aerosols and contribute to PM concentrations biases.

We evaluate EXP4 with observed surface aerosol concentrations, and across all sites the model underestimates observed  $PM_{10}$  by  $\sim 25\%$  (model average  $7.5\text{ }\mu\text{g m}^{-3}$  compared to IMPROVE average of  $10.1\text{ }\mu\text{g m}^{-3}$ ), with some sites indicating greater differences ( $\sim 35\%$  in CBL and ELI). One potential reason for the  $PM_{10}$  discrepancy is that our simulations only include “anthropogenic dust” from the US-NEI, and we do not simulate meteorologically driven dust within WRF-Chem. In contrast, across all sites the modeled  $PM_{2.5}$  is underestimated by  $\sim 8\%$  (model average of  $6.1\text{ }\mu\text{g m}^{-3}$  compared to the measurement average of  $7.0\text{ }\mu\text{g m}^{-3}$ ).  $PM_{2.5}$  is associated with the emissions from urban regions, dominated mainly by the anthropogenic emissions from urban areas such as Oklahoma City, Tulsa, and Kansas City. There are several sites where  $PM_{2.5}$  is overestimated by the model (TAL, CBL, and ELI) that also simulate an overestimation in  $PM_{10}$ .

### 3.2. Temporal Evolution of Primary and Subpollen Particles

Averaged over the entire model domain, Figure 4 shows the temporal variations of column averaged POLP and POLS for the five different sensitivity tests (EXP1 to EXP5) along with rainfall and total (IC + CG) lightning

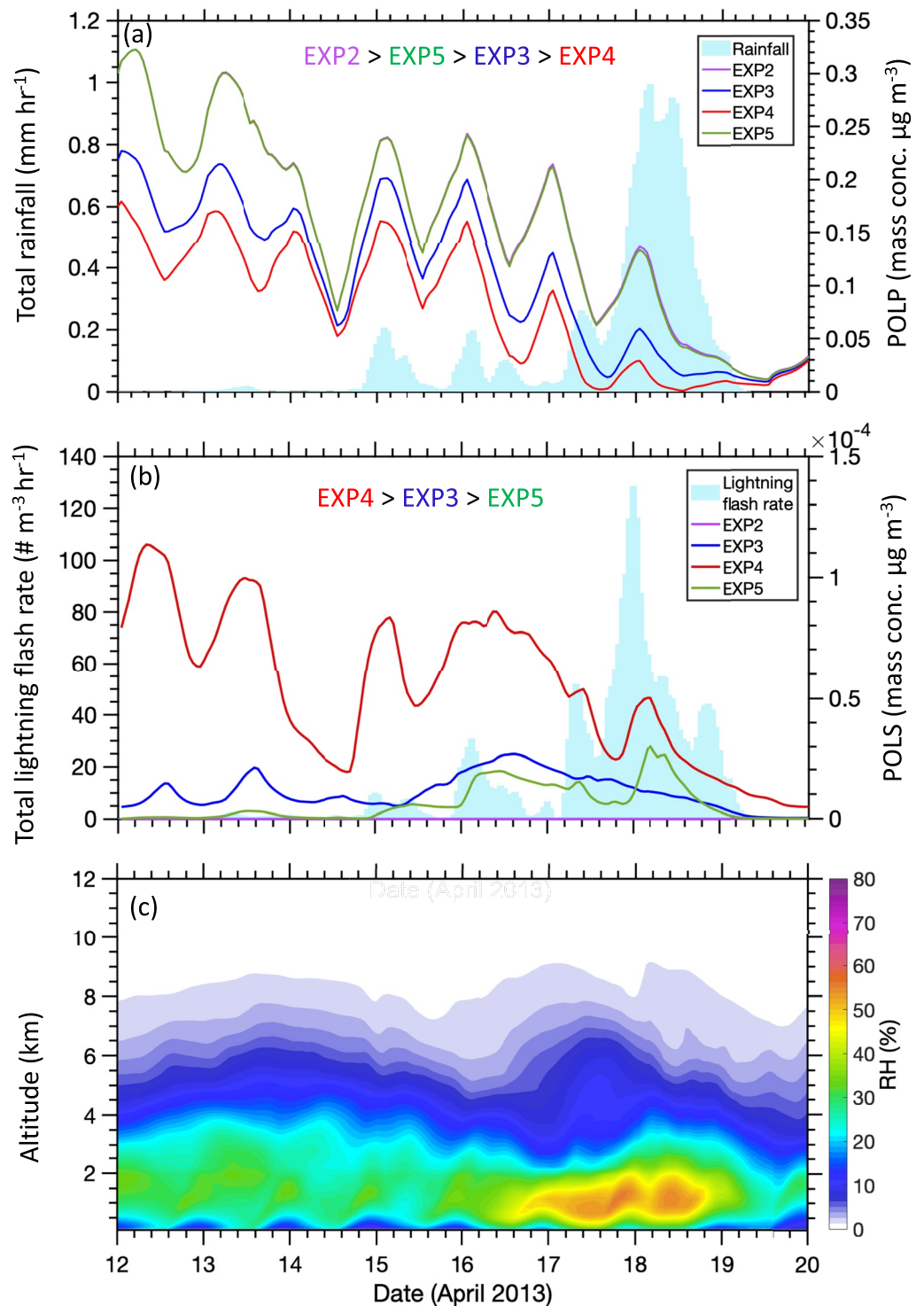


**Figure 4.** Temporal evolution of column averaged hourly (a) primary pollen (POLP), and (b) subpollen (pollen and subpollen) pollen mass concentration (solid-colored lines) averaged over the entire model domain (right axis). Light blue bars indicate the average hourly rainfall (a) and cloud mixing ratio (b) (left axis). Each experiment line is the average of the three ensemble members of the respective experiments. (c) Temporal evolution of vertical profiles of hourly averaged relative humidity (RH %).

flash rates. In addition to the impacts of wind and humidity, the pollen loading is affected by rain (Equation 4). The reduction of POLS and POLP in the second half of the simulation (after 16 April) are due to the removal of both coarse and fine aerosol by precipitation (domain averaged rainfall  $>0.5 \text{ mm hr}^{-1}$ ). Relative humidity and lightning directly influence the generation of the POLS (Figures 4b and 4c). The vertical profiles of relative humidity (RH %) averaged over the domain show the highest values between April 17–19 (Figure 4c). The surface and atmosphere humidity-induced rupture causes POLS to increase with moist conditions, resulting in high columnar POLS in both EXP3 (surface) and EXP4 (surface + in atmosphere). Similarly, EXP5 (cloud-to-ground + in-cloud lightning) shows higher rupture when flash rates increase (Figure 4b). Over the simulation, the averaged columnar POLS in EXP5 is much lower than in EXP3 and EXP4 even when lightning increases between 17 and 19 April. Comparing all the experiments, the production of POLS is the greatest for EXP4, followed by the surface rupture in EXP3, with the lowest concentration of POLS produced by the lightning rupture (EXP5). POLP increases when POLS formation is low, and the most primary pollen is present in EXP2 with no rupture, followed by the lightning rupture (EXP5) and the two humidity-induced rupture experiments (EXP3 and EXP4). In Section 3.3, we provide further details on the variations of pollen in the atmosphere for these five experiments.

Using EXP5 (lightning-induced pollen rupture) as an example, we compare the spatial distribution of POLP and POLS with pollen loading-dependent meteorological parameters, including rainfall, cloud fraction, and lightning flash rates (Figure 5). Here we evaluate 24-hr averages of pollen in the lowest 5 km for three days that show the evolution of pollen rupture with meteorological conditions. On the first day (12 April), dry atmospheric conditions and low lightning activity lead to high POLP emissions and low POLS generation (Figure 5a). Following Equation 2, pollen loadings are directly proportional to the wind magnitudes over the region. Wind direction further influences the transport of POLP and POLS, with strong south-easterlies carrying POLP away from the south-eastern part of the domain where the pollen emission fluxes are at a maximum (Figure 2a). The first day simulates higher POLP (up to  $3 \mu\text{g m}^{-3}$ , Figure 5a) with low cloud fractions (up to 0.1, Figure 5b) and a lack of rain and lightning (Figure 5c), leading to very low POLS ( $<1\text{e}^{-6} \mu\text{g m}^{-3}$ , Figure 5b). On 15 April, POLS increases in the northeastern part of the domain (Figure 5e) due to an increase in lightning activity (Figure 5f) and rainfall (Figure 5f). As the convective activity builds on 18 April, the increase in lightning activity increases the POLS generation (coincident with the IC-flash rate) and the wind carries the pollen toward the center of the domain, creating a convergence zone within the convective system. Hence, a strong band of convective activity in the eastern half of the domain reduces POLP (now  $<1 \mu\text{g m}^{-3}$ , Figure 5g) and increases the accumulation of POLS (up to  $5\text{e}^{-6} \mu\text{g m}^{-3}$ , Figure 5h) corresponding to the heavy lightning activity (Figure 5i).

We further select two regions (R1 and R2) to delineate the processes involved in pollen evolution. R1 has a higher POLS loading (Figure 5h) and is relatively cloudy, with heavy rainfall toward the end of the simulation (Figure 5i). In contrast, R2 has a relatively lower pollen load (Figure 5h) and weaker precipitating cloud (Figures 5f and 5i). Both R1 and R2 experienced an average lightning flash rate of  $\sim 0.06 \text{ \# km}^{-2} \text{ hr}^{-1}$  during the convective activity on 18 April, influencing the generation of POLS. Overall, this progression of a convective system indicates how meteorological conditions evolving from dry conditions with high POLP emissions can lead to increased rupture events as POLP interacts with convective systems.

### 3.3. Vertical Distribution of Primary and Subpollen Particles

To understand the transport of POLP in the atmosphere and where POLS is formed in the atmospheric column, we examine the vertical distribution of POLP and POLS (Figure 6) in the two regions outlined in Figure 5a. R1 has higher pollen concentrations than R2, as a result of the distribution of primary pollen (Figures 6a–6d and 6h–6k respectively) and higher formation of POLS due to high humidity and lightning activity (R1: Figures 6e–6g; R2: Figures 6l–6n). Physical properties of POLP and POLS influence the horizontal and vertical transport, where the smaller and lighter POLS have lower settling velocities that allow them to be transported to higher altitudes and longer distances. Generally, POLP and POLS concentrations decrease with altitude, except for the high convective periods. POLP concentrations reach up to  $1 \text{ mg m}^{-3}$  throughout the first 8 km when rupture processes are absent or minimal (e.g., EXP2 and EXP5) with reductions during the atmospheric humidity-rupture periods (EXP4) and accompanied by the highest concentration of POLS. POLP is greatest near the surface of R1, which experiences more rainfall and cloud cover and higher emissions, with mass concentrations reaching up to  $1 \text{ mg m}^{-3}$  (equivalent to  $\sim 200$  primary pollen grains  $\text{m}^{-3}$ ). During the non-convective days in the earlier part of the simulation



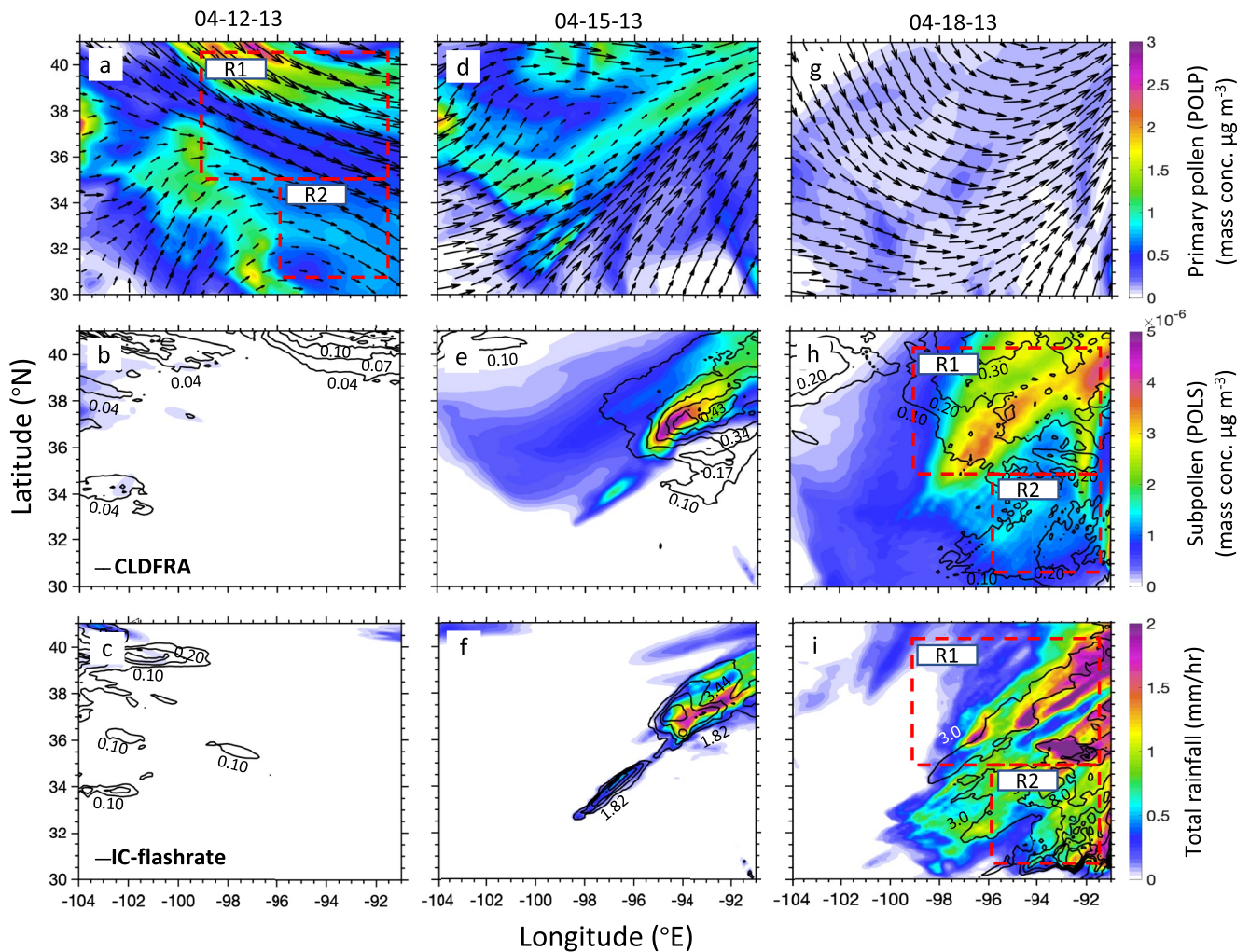


**Figure 5.** Spatial distribution of (a, d, and g) primary pollen (POLP) (color-filled contours) and wind vectors, (b, e, and h) subpollen (pollen and subpollen) (color-filled contours), and cloud fraction (CLDFRA) (open contours) and, (c, f, and i) total rainfall (color-filled contour), and in-cloud lightning flash rates (open contours). Boxes in each row show two regions of interest (R1 and R2). Each column represents 12, 15, and 18 April 2013, respectively.

(12–16 April), POLP grains are well-mixed within the first 5 km and, in some instances, above 5 km. During the high convection days (17 and 18 April), POLP is transported to a height of approximately 12 km in the atmosphere, suggesting that pollen can be mixed throughout the free troposphere. In contrast, POLP and POLS are much lower over R2, with their vertical distributions not exceeding 5 km.

Figure 6 highlights the differences in rupture processes that drive the formation of POLS. In EXP2 where rupture is not included (Figures 6a and 6h), POLP remains high until 16 April, after which the wet removal decreases atmospheric concentrations. Due to the absence of rupture, POLP in EXP2 remains higher throughout the simulation period than in other simulations. Apart from the wet removal, POLP further decreases in EXP3 and EXP4 (humidity-induced rupture experiments) due to the formation of POLS in the second half of the simulation. Similarly, the generation of POLS due to the lightning-induced rupture is apparent in EXP5 (Figures 6g and 6n). Surface-only rupture (EXP3) simulates lower POLS concentration compared to EXP4 due to the lack of in-atmosphere rupture events. The surface-only induced humidity rupture of EXP3 (Figures 6e and 6l) creates less POLS ( $<1.0 \times 10^{-4} \text{ mg m}^{-3}$  or  $\sim 4 \times 10^4$  subpollen grains  $\text{m}^{-3}$ ), and POLS is generally confined to  $\sim 3$  km and reaches  $\sim 6$  km during highly convective hours. However, the addition of in-atmospheric rupture (EXP4; Figures 6f and 6m) increases POLS below 5 km, with its mass concentration reaching up to  $2 \times 10^{-4} \text{ mg m}^{-3}$  (or  $\sim 8 \times 10^4$  subpollen grains  $\text{m}^{-3}$ ). Interestingly, even on highly convective days, surface humidity rupture-only processes (EXP3, Figure 6e) are not able to transport POLS to the higher altitudes (up to 12 km) as in the case

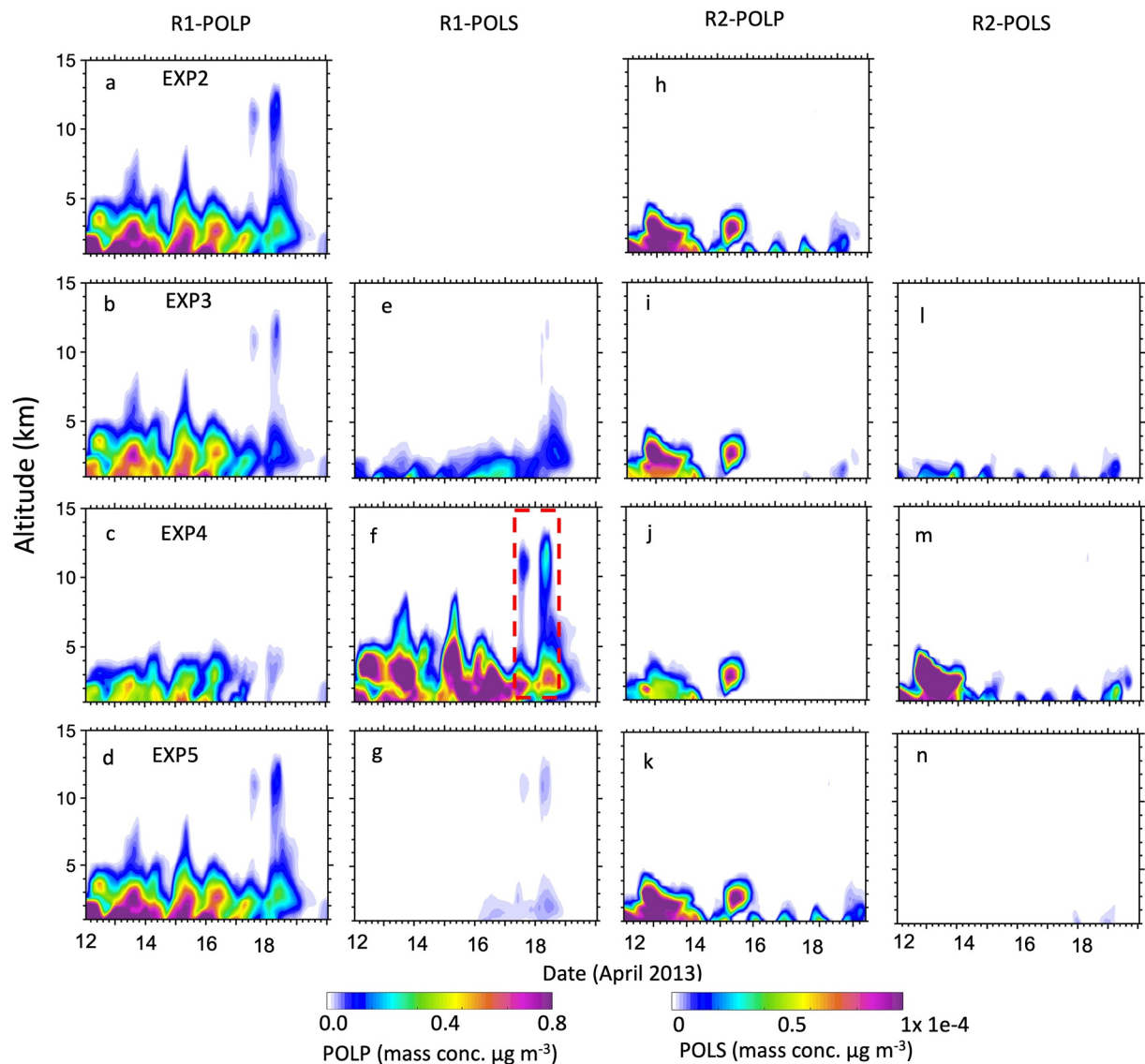


**Figure 6.** Temporal evolution of vertical profiles of hourly averaged primary pollen (POLP) and subpollen (pollen and subpollen) mass concentration from the three ensemble members of different experiments (EXP2 in row 1, i.e., a and h; EXP3 in row 2, i.e., b, e, i, and l; EXP4 in row 3, i.e., c, f, j, and m; EXP5 in row 4, i.e., d, g, k, and n), averaged over region R1 (columns 1 and 2) and R2 (columns 3 and 4). The red-dotted box in “f” highlights the time of high thunderstorm activity.

of EXP4 (Figure 6f), suggesting that in-atmosphere rupture has a strong influence on free troposphere pollen concentrations.

For EXP5, IC and CG lightning rupture POLP throughout the atmosphere, resulting in the formation of POLS ( $\sim 0.1e^{-4} \text{ mg m}^{-3}$  or  $\sim 4e^3$  subpollen grains  $\text{m}^{-3}$ ). Pollen and subpollen production is consistent with the lightning activity (Figure 6g), which peaks during the thunderstorm event on 17 and 18 April. During the peak lightning period, the in-cloud (from 8 to 12 km) rupture of primary pollen results in high values of POLS production ( $\sim 0.3e^{-4} \text{ mg m}^{-3}$  or  $\sim 1.2e^4$  subpollen grains  $\text{m}^{-3}$ ), like that of high humidity in-atmosphere rupture in EXP4 but with a much lower magnitude. We note that the relatively low POLS in EXP5 compared to EXP3 and EXP4 could be because of the low conversion fraction ( $F_{\text{rupt}} = 0.1$ ) from POLP to POLS (Equation 7). An additional simulation was performed with the lightning flash rate factor increased by 20 times as a sensitivity analysis, which increased POLS production by  $>80\%$  (not shown). This increase in the lightning flash rate is not consistent with observed lightning flash counts (Barth et al., 2014; Zhu et al., 2019), but we note that an increase in either the flash count or the rupture rate ( $>10\%$ ) would act to increase the contribution of POLS from lightning. At a 12 km horizontal resolution, we would not expect that a single lightning flash would rupture all the POLP within



that grid cell, although we note that the 10% value used in these simulations is extremely uncertain. Our current lightning rupture experiment (EXP5) has significantly lower POLS than EXP3 and EXP4 over the less convective region R2 with very low lightning activity (Figure 6n).

### 3.4. Vertical Lifting of Primary and Subpollen Particles During Thunderstorm and Lightning Events

To understand the processing of pollen within a thunderstorm, Figure 7 (EXP5) and 8 (EXP4) illustrate the various stages of development and decay of a thunderstorm cell and the associated rainfall, temperature, and vertical velocity averaged over the latitudinal range 36–37°N, which includes the area of high pollen loading at higher altitudes (also shown in Figure 6f). The thunderstorm organization in the SGP is strongly coupled to changes in large-scale wind and moisture patterns, and the model simulates thunderstorm events on 17 and 18 April 2013. On these two days, an unstable air mass was observed across Oklahoma and southern Kansas, resulting in multiple thunderstorms in this region (<https://www.spc.noaa.gov>). One of the main drivers for this thunderstorm activity is the nocturnal LLJ stream (Bedka & Mecikalski, 2005). The storm cells formed at the intersection of the eastward cold front with warm, moist southerly flow from the LLJ.

The thunderstorm generates a series of updrafts starting in the evening (~21:00 hr, Figures 7a and 8a) on 17 April and lasting until the early morning hours (03:00, Figures 7d and 8d) of the following day. This thunderstorm is accompanied by heavy rain (up to 14 mm hr<sup>-1</sup>, Figures 7g and 8g) and a strong temperature contrast near the surface (around -99 to -97°E, Figures 7 and 8). The cold air mass from the west replaces the warm air being lifted during the event, in conjunction with downdrafts from the convective events results in a cold pool at the backside of the thunderstorm (at approximately -97°E) at ~20:00 hr on 17 April. The strong temperature contrast during the night further accelerates the jet (Bedka & Mecikalski, 2005; Fedorovich et al., 2017), and strong low-level wind shear starts to build within an hour, creating a large thunderstorm in the next few hours (23:00 on 17 April to 01:00 on 18 April; Figures 7b, 7c, 8b, and 8c). The vertical shear is accompanied by low-level moisture advection, creating an anvil that extends along the direction of the upper-tropospheric winds. The continuous vertical wind shear favors the persistence of the thunderstorm event.

The thunderstorm decay process begins roughly 8 hr later (03:00 on 18 April; Figure 7d), accompanied by early morning precipitation. This activity transports warm, moist air, which further fuels the thunderstorm and disappears early in the morning as the sun rises and the LLJ stream dissipates. Lightning is associated with the event (e.g., Figures 7b and 8b), and IC and CG lightning activity ruptures POLP, causing POLS to spread throughout the upper atmosphere in EXP5 (Figure 7c). Further, the strong convective activity lifts the POLS to higher altitudes of ~12 km, where POLS accumulates up to ~2e<sup>-4</sup> μg m<sup>-3</sup> in the anvil with high lightning activity.

Similarly, EXP4 shows that high humidity within and surrounding the thunderstorm along with the high convective activity results in high POLS formation up to ~4e<sup>-4</sup> μg m<sup>-3</sup> (Figure 8). Comparing EXP4 and EXP5, the POLS generated in EXP4 is higher in magnitude than EXP5 by ~80% throughout the atmosphere. However, the vertical temperature perturbation is similar in both cases, and a high vertical wind shear develops around -98° to -94°E, which is associated with the warm air lifting, resulting in moisture advection and further storm development.

During the thunderstorm evolution, vertical updrafts of ~2 m s<sup>-1</sup> (averaged over 12 km) lifts POLP and POLS to the upper troposphere (10–12 km) and transports the ruptured pollen (POLS) laterally in the anvil outflow. Due to the coarser horizontal resolution utilized in these simulations (12 km), our simulations of updrafts and downdrafts may be simplified. Vertical updrafts carry POLP into the cloud, where the high humidity in EXP4 causes further rupture of POLP at the higher altitudes. These events are accompanied by rainfall and lightning activity, allowing the pollen to rupture. The IC and CG lightning strikes rupture the lifted POLP at higher altitudes (~12 km). As shown in Figures 7 and 8, vertical updrafts (~2 m s<sup>-1</sup> -averaged over 12 km) are sufficient to loft pollen to the upper troposphere (up to ~12 km). On days with little to no convective activity (20:30 on 13 April, 02:30 on 17 April; updrafts <1 m s<sup>-1</sup>), pollen is only present up to altitudes of 4–7 km (Figure 6). This suggests that for pollen rupture to occur within a thunderstorm, the vertical temperature difference and the associated instability and wind shear are important factors. Additionally, the horizontal anvil and solid horizontal winds can increase the likelihood of long-distance transport of POLP and POLP. While we do not test both the humidity and lightning induced rupture together, these results suggest that a mature thunderstorm, characterized by intense lightning activity and precipitation, can rupture POLP and further aid in the distribution of pollen.

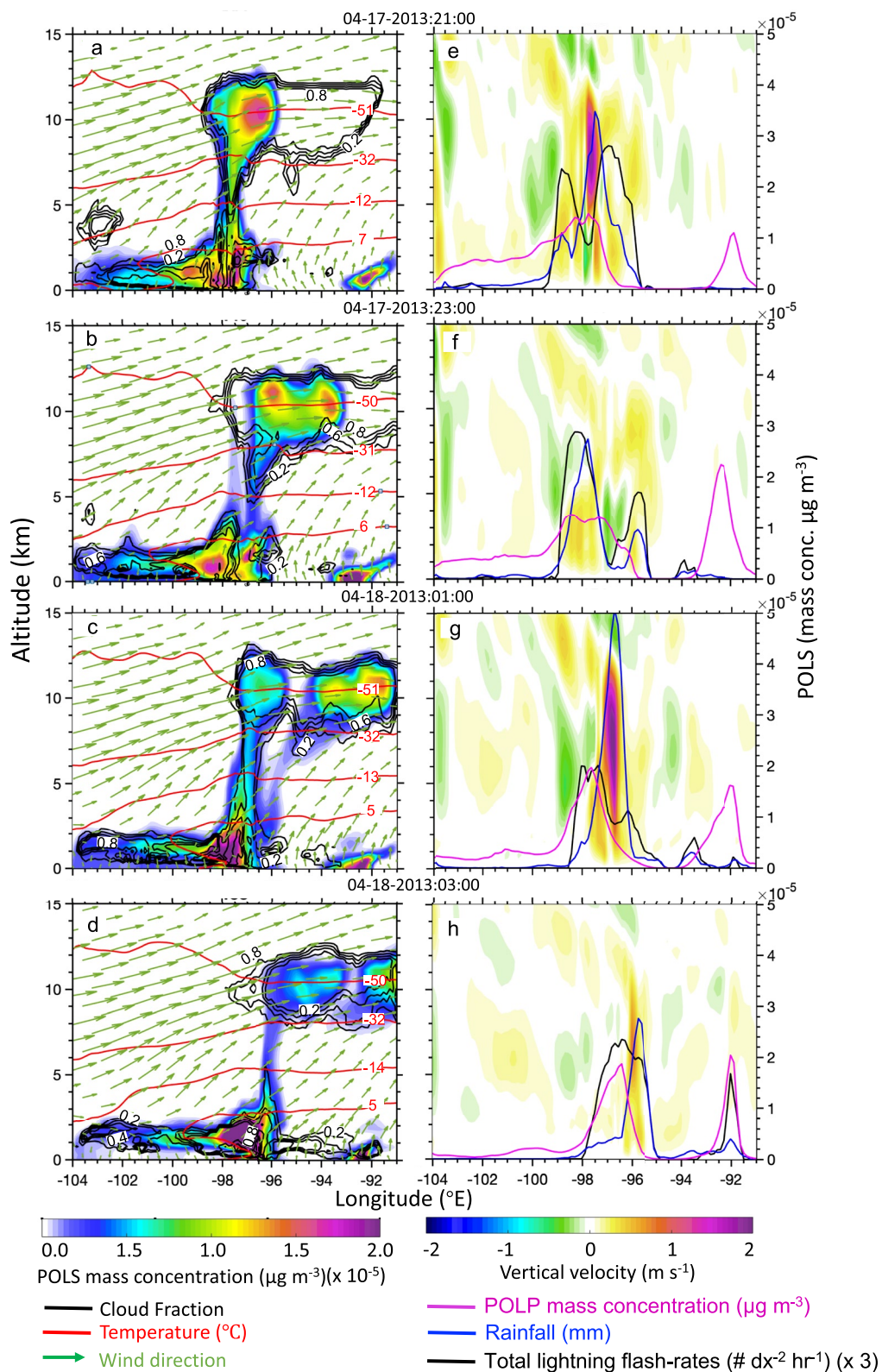


**Figure 7.** Horizontal cross section of the stages of development and decay of a thunderstorm cell and associated lightning activities as simulated by EXP5 for (a to d) pollen and subpollen (color contours;  $\mu\text{g m}^{-3}$ ), wind vectors, cloud fraction (black open contours), and temperature (red open contours,  $^{\circ}\text{C}$ ); (e to h) vertical velocity (color-filled contours;  $\text{m s}^{-1}$ ), and the total lightning flash rates (black lines), respectively rainfall (blue line;  $\text{mm hr}^{-1}$ ), and column averaged POLP mass concentration ( $\mu\text{g m}^{-3}$ ).

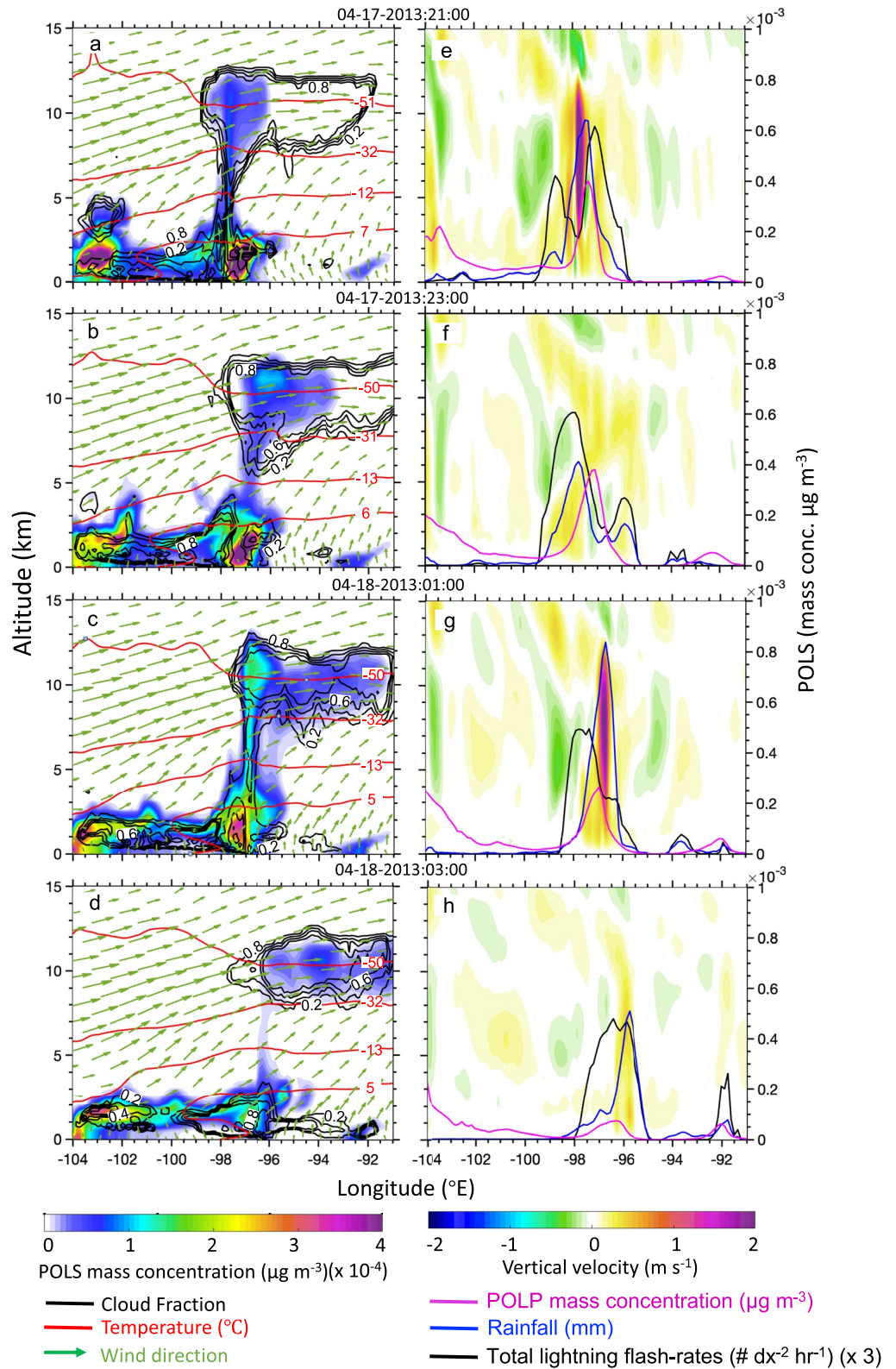


**Figure 8.** Horizontal cross section of the stages of development and decay of a thunderstorm cell and associated lightning activities as simulated by EXP4 for (a to d) pollen and subpollen (color contours;  $\mu\text{g m}^{-3}$ ), wind vectors, cloud fraction (black open contours), and temperature (red open contours,  $^{\circ}\text{C}$ ); (e to h) vertical velocity (color-filled contours;  $\text{m s}^{-1}$ ), and the total lightning flash rates (black lines, respectively) rainfall (blue line;  $\text{mm hr}^{-1}$ ), and column averaged POLP mass concentration ( $\mu\text{g m}^{-3}$ ).



### 3.5. Impact of Pollen on Hydrometeors

Finally, we examine the impact of pollen on cloud formation and hydrometeor evolution. Figure 9a shows the vertical distribution of the hydrometeors during high convection days (17 and 18 April 2013) alongside differences between the experiments with pollen (EXPs 2 to 5) and the ones without pollen (EXP1) (Figure 9b). Our analysis focuses on R1, where pollen concentrations and convective activity are higher than in R2. Hydrometeors vary negligibly with pollen loading in region R2 (figure not shown).

We analyze vertical profiles of five hydrometeors, including cloud, ice, snow, rain, and graupel, and the impact of pollen on these hydrometeors. The vertical distribution of cloud water mixing ratio (QCLOUD) decreases with the addition of pollen by  $\sim 5\%$  below 4 km, where the mixing ratios are the largest ( $7e^{-2} \text{ g kg}^{-1}$ ) (Figures 9a and 9b). Decreases in QCLOUD are greatest in EXP4, which had the greatest amount of rupture and POLS formation, followed by EXP3, with little change in the low-rupture lightning experiment (EXP5) and the simulation without rupture (EXP2). These results suggest that the rupture processes have a minor influence on cloud water within the low cloud layer. However, this may depend on grid cell resolution (Brient et al., 2015; Vial et al., 2016, 2017). On the other hand, along the low cloud layer, QVAPOR increases by  $\sim 2\%$  with the addition of pollen below 2 km (with negligible changes aloft) consistent with the QCLOUD decreases (i.e., the greatest increase is in EXP4, followed by EXP3 and EXP5). The decrease in the cloud water is compensated by the direct rain collection and the increase in QRAIN by  $\sim 2\%$ . The increase in perturbation potential temperature also shows a similar relationship, with warmer perturbation temperatures scaling with the POLS and reduced QCLOUD (not shown).

In the current model configuration, ice phase hydrometeors are only estimated from temperature-dependent ice nucleation parameterizations (Meyers et al., 1992) and are not influenced by aerosol number concentrations. The ice phase hydrometeors reveal several small changes depending on the rupture experiment, likely driven by changes in thermodynamic properties. In all experiments, graupel (QGRAUPEL) and snow water (QSNOW) mass mixing ratios maximize between 5 and 8 km, while ice water (QICE) peaks slightly higher between 9 and 11 km. Experiments with lower rupture rates (EXP2, EXP3, and EXP5) lead to relatively higher POLP compared to EXP4 (aloft, Figure 6), which has more POLS throughout the atmospheric column. Generally, the greatest changes in cold phase hydrometeors are for graupel and snow. Changes to QICE are relatively small, generally showing slight increases at the altitude of peak mixing ratio ( $\sim 10$  km) and slight decreases above and below this altitude and are not outside of the model standard deviation, indicating that they are not statistically significant.

Overall, for experiments with lower POLS, both QGRAUPEL and QSNOW show a slight increase of ( $\sim 2\% - 5\%$ ). In contrast, EXP4 which has the greatest rupture simulates a slight decrease of  $\sim 2\%$  of QSNOW and a negligible change in QGRAUPEL. Similar for QICE, EXP4 shows the maximum change with an increase of  $\sim 2\%$ . The experiments with low POLS (EXP3 and EXP5) leads to the highest positive response of QSNOW and QGRAUPEL ( $\sim 5\%$ ) over the altitudes 7–8 km due to lower conversion from ice water mixing ratio (QICE). However, all the experiments show increasing ice phase hydrometeors aloft ( $> 10$  km). Graupel and snow mass mixing ratios are controlled by several processes, including formation processes as well as loss processes through collision with and collection by other hydrometeors. Because both graupel and snow increases generally greatest for the lower POLS simulations (e.g., EXP2, EXP3, and EXP5), we postulate that greater POLS can lead to greater rain rates, which then may reduce the snow and graupel mass. Using the standard deviation values of the ensemble members, these changes to QCLOUD, QGRAUPEL and QSNOW are greater than the model ensemble spread, suggesting that they are significant changes. These simulations did not allow POLP or POLS to act as INP, therefore, any changes to the cold cloud phases would be due to changes in thermodynamics as a result of warm cloud processes. We plan to revisit this with the updated aerosol-aware INP parametrization.

## 4. Summary and Conclusions

Primary pollen emission is a function of the vegetation type and meteorological factors that drive emission, including relative humidity, wind, and rainfall. Primary pollen grains from vegetation can rupture to subpollen at the surface or in the atmosphere due to high humidity and/or lightning activity. This study includes primary pollen emissions and their atmospheric rupture processes within a coupled aerosol-meteorology model to investigate how pollen is transported in the atmosphere before, during, and after a convective event in the US Central Great Plains.

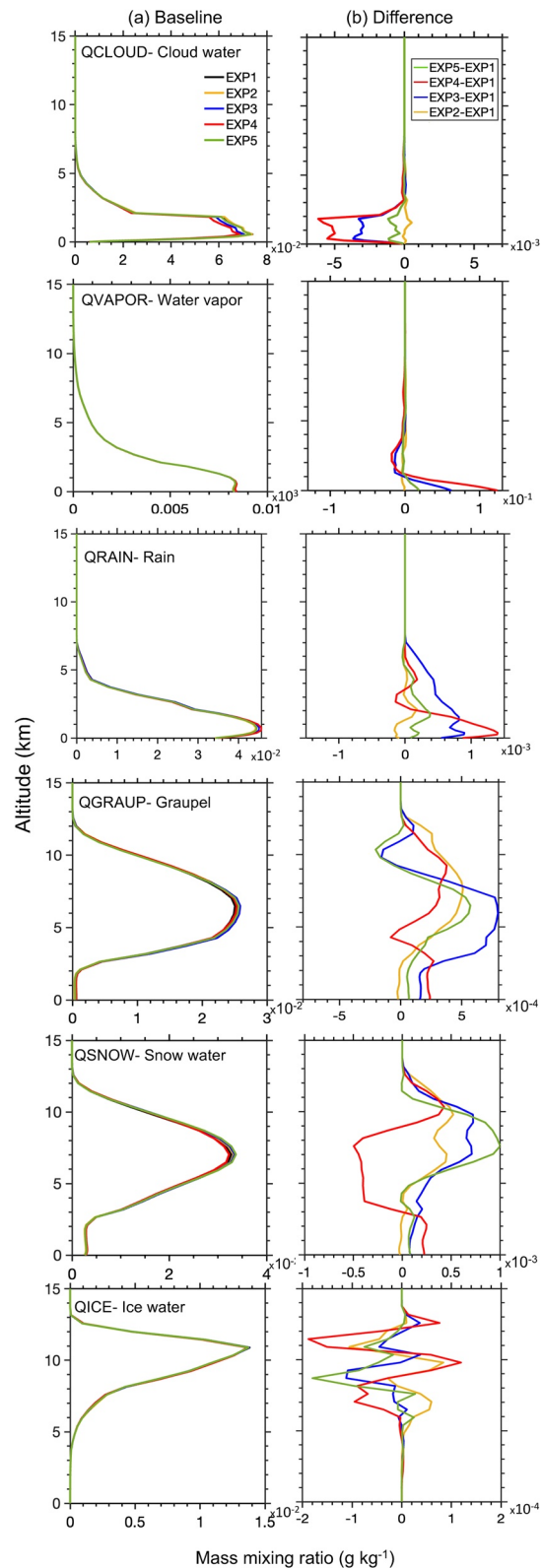


**Figure 9.** Vertical distribution of (a) hydrometeors including cloud water (QCLOUD), water vapor (QVAPOR), rain (QRAIN), graupel (QGRAUP), snow water (QSNOW), and ice water mixing ratio (QICE) for EXP1 to 5, and (b) hydrometeor difference (EXP2to5 – EXP1) averaged over region R1, during 17–18 April.



A new module for pollen within the MADE-SORGAM framework in the WRF-Chem model adds two new aerosol tracers (POLP for primary pollen and POLS for subpollen) to represent aerosol species of biological origin. The pollen module runs parallel with other aerosol emissions, including biomass-burning, sea salt, and dust. The PECMv2.0 model provides the total pollen emission potential. The pollen module couples the pollen emission fluxes with the online meteorology and converts POLP to POLS via various rupture mechanisms. Both pollen tracers are subject to all major atmospheric processes, including transport, gas-aqueous-phase chemistry, influence on radiative properties and cloud formation, and wet and dry deposition.

We conduct a suite of ensemble runs that simulate POLP and three different pollen rupture mechanisms that generate POLS, including:

1. high humidity or precipitation induced surface rupturing (EXP3),
2. in-atmosphere plus surface rupturing (EXP4), and
3. Lightning-induced rupturing, where in-cloud and cloud-to-ground lightning strikes trigger pollen rupture events based on the WRF-Chem lightning parametrization (EXP5).

Rupture of the POLP at the surface and in the atmosphere (EXP4) maximizes during the high humidity conditions such as the thunderstorms simulated in the SGP model domain, resulting in higher POLS from this rupture process than the other rupture mechanisms. Lightning induced rupture (EXP5) simulates higher atmospheric (cloud-to-ground and in-cloud) rupture during lightning activity. However, the magnitude of the production of POLS from lightning (EXP5) is much lower (by 90%) than rupture induced by humidity (EXP4), though we note that the conversion rate of POLS in these events is highly uncertain.

Figure 10 summarizes the pollen transport within a thunderstorm, as represented by the humidity-induced rupture simulation (EXP4). The thunderstorm period begins late on 17 April 2013 and matures in the early hours of 18 April 2013. Strong low-level wind shear creates a large thunderstorm within several hours, further accelerating the jet and increasing the vertical temperature gradient. The high convective activity allows both primary and subpollen to mix throughout the boundary layer (Figures 10a and 10b) and transport through the troposphere via the vertical updrafts (Figure 10b). The vertical shear and low-level moisture advection creates an anvil that extends along the direction of the upper-tropospheric winds. Under these convective conditions, the vertical updraft lifts subpollen to the upper troposphere (10–12 km) and transports it laterally in the anvil outflow, which is enhanced in the matured stage of the storm (Figure 10b).

Overall, the pollen spatial and temporal distribution depends on their emission potential and the ambient meteorological conditions. Vertical wind shear is also responsible for lifting pollen to higher altitudes as a result of strong convection, as shown by the relatively low subpollen concentrations at higher altitudes (>8 km) in the first half of the simulation where deep convection is not evident (Figure 10a; before 16 April) and increased subpollen concentrations above 8 km during the convective periods (after 16 April; Figure 10b).

This analysis of pollen rupture has implications for our understanding of thunderstorm asthma. Atmospheric processes have several possible mechanisms for rupturing pollen, with potential return of ruptured pollen particles via downdrafts and horizontal transportation via the anvil outflow. There are two potential mechanisms for ruptured pollen aloft to be returned to the surface, either via the rear-flank downdraft (RFD) or the forward-flank downdraft (FFD). In Figure 10, the rear-flank downdrafts (RFD) are higher (up to  $0.4 \text{ m s}^{-1}$  in both the early and mature stages of the storm) than the forward-flank downdraft (FFD; not present in the early stage but increasing up to  $0.16 \text{ m s}^{-1}$  in the mature stage). RFD are typically associated with a strong temperature contrast near the surface and are created by dry upper-level winds impinging on the backside of the storm. The strong wall of the vertical updraft at the convective core and RFD together act as a barrier for the vertical transport of POLP to higher altitudes (Figure 10b), and instead humidity-induced rupture in the lower atmosphere converts POLP to POLS and carries them upward along with the vertical updraft in the convective core. The RFD restricts the pollen from rising upwards at the back of the storm and increases near surface concentrations. The RFD and the vertical updraft region are associated with precipitation (Figure 9), which further suppresses the POLP and aids the generation of POLS. The FFD is weaker than the RFD, but it does increase in strength during the mature stage (Figure 10b). In these simulations, we do not simulate pollen being transported by the FFD from the high altitudes to the surface, although this may be limited by the resolution of the model (12 km). However, we notice a slight downward transport of POLS between 8 and 10 km (Figure 10b) along with the FFD (around  $95.5^\circ\text{E}$ ), although

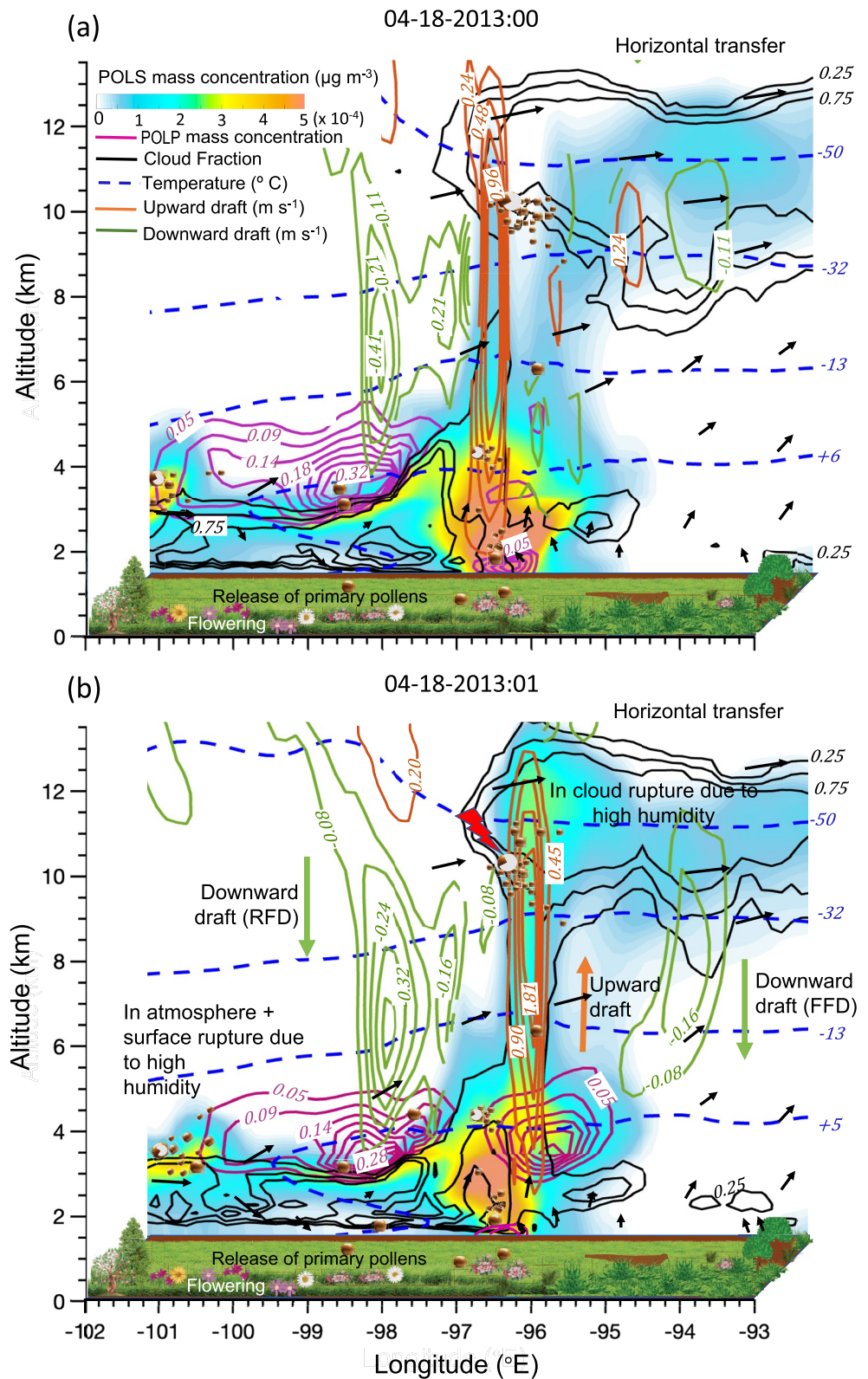


**Figure 10.** Summary schematic of the pollen rupture mechanisms, enhancement, and transfer during and the role of the convective activities during (a) the initial stage and (b) the mature stage of thunderstorm simulated in EXP4. Here rear-flank downdraft (RFD) and forward-flank downdraft (FFD) indicate RFDs and FFDs, respectively.

this does not appear to reach all the way to the surface. A north-westward wind direction may restrict the downdraft and carry the POLS outside of the simulation domain.

Additionally, the resolution and domain size cannot precisely track the extension of the horizontal anvil and the potential return of POLS to the surface from the anvil outflow. Despite the resolution limitations, these results suggest that the recirculation of POLS to the surface from the upper anvil may not be possible in the local sense, however, this may occur further downwind of the convective event. From these results, we postulate that much of the subpollen generated during thunderstorm events is occurring due to humidity-driven rupture within the boundary layer, as the downdrafts do not seem capable of returned pollen ruptured aloft to the surface.

Finally, we evaluated the effect of these particles on cloud formation and hydrometeor evolution during a thunderstorm with lightning. The cloud, snow, and graupel mixing ratio were slightly affected by the presence of pollen (changes of about <5%) during the highly convective days. The remaining hydrometeors show weak responses (<2%) to POLP and POLS. However, we note that we only include pollen as a CCN, and not as an ice nucleating particle in the cloud-microphysics process as this was beyond the scope of the current study. Future work will consider the role of POLS and POLP as INP using new laboratory measurements, which will be important to understand the role of PBAP in the cloud formation process.

Although these uncertainties remain, this manuscript illustrates the implementation of a newly developed pollen module in WRF-Chem which simulates primary pollen and atmospheric-driven pollen rupture that produces subpollen at the surface and in the atmosphere. The spatial and temporal distribution of pollen is related to its emission potential and the meteorological conditions, with pollen being lifted to the upper troposphere (10–12 km) during the vertical updrafts and transported laterally in the anvil top outflow. Our sensitivity simulations suggest that the lightning rupture mechanism generates fewer subpollen than the surface and in atmosphere rupture during high humidity during events in the Central United States and this may be important for forecasting future events of pollen rupture and thunderstorm asthma.

## Data Availability Statement

The Weather Research and Forecasting Model with Chemistry model code is available from ([www2.mmm.ucar.edu/wrf/users/download/](http://www2.mmm.ucar.edu/wrf/users/download/)). WRF-Chem preprocessors are available on the website ([www.acom.ucar.edu/wrf-chem](http://www.acom.ucar.edu/wrf-chem)). Pollen emissions based on Y. Zhang and Steiner (2022) are available from [https://deepblue.lib.umich.edu/data/concern/data\\_sets/0c483j691?locale=en](https://deepblue.lib.umich.edu/data/concern/data_sets/0c483j691?locale=en). The model output data are made available upon request. The primary tools to analyze the model output and generate figures are cdo ([code.mpimet.mpg.de/projects/cdo/](http://code.mpimet.mpg.de/projects/cdo/)) and MATLAB ([www.mathworks.com/products/](http://www.mathworks.com/products/)). Observed aerosol data is available from The IMPROVE ([vista.cira.colostate.edu/Improve/improve-data/](http://vista.cira.colostate.edu/Improve/improve-data/)) and the US EPA ([www.epa.gov](http://www.epa.gov)). The severe weather event report by the Storm Prediction Center of NOAA's National Weather Service is available at the website ([www.spc.noaa.gov/](http://www.spc.noaa.gov/)).

## Acknowledgments

This research was primarily supported by the U.S. Department of Energy's Atmospheric System Research, an Office of Science Biological and Environmental Research program, under Grant DE-SC0019084. Additional support for pollen emissions modeling by Y.Z. was provided by National Science Foundation Grant AGS-1821173. PM<sub>10</sub> data were graciously provided by United States Environmental Protection Agency, PM<sub>10</sub> and PM<sub>2.5</sub> by seven IMPROVE. IMPROVE is a collaborative association of state, tribal, and federal agencies, and international partners. US EPA is the primary funding source, with contracting and research support from the National Park Service. The Air Quality Group at the University of California, Davis is the central analytical laboratory, with ion analysis provided by Research Triangle Institute, and carbon analysis provided by Desert Research Institute. Storm Prediction Center of NOAA's National Weather Service provided the severe weather event report which identified the severe storm days. The authors would like to acknowledge high-performance computing support from Cheyenne provided by NCAR's Computational and Information Systems Laboratory.

## References

- Ackermann, I. J., Hass, H., Memmesheimer, M., Ebel, A., Binkowski, F. S., & Shankar, U. (1998). Modal aerosol dynamics model for Europe: Development and first applications. *Atmospheric Environment*, 32(17), 2981–2999. [https://doi.org/10.1016/S1352-2310\(98\)00006-5](https://doi.org/10.1016/S1352-2310(98)00006-5)
- Andreae, M. O., & Rosenfeld, D. (2008). Aerosol–cloud–precipitation interactions. Part 1. The nature and sources of cloud-active aerosols. *Earth-Science Reviews*, 89(1), 13–41. <https://doi.org/10.1016/j.earscirev.2008.03.001>
- Andrew, E., Nehme, Z., Bernard, S., Abramson, M. J., Newbiggin, E., Piper, B., et al. (2017). Stormy weather, a retrospective analysis of demand for emergency medical services during epidemic thunderstorm asthma. *British Medical Journal*, 359, j5636. <https://doi.org/10.1136/bmj.j5636>
- Anenberg, S. C., Weinberger, K. R., Roman, H., Neumann, J. E., Crimmins, A., Fann, N., et al. (2017). Impacts of oak pollen on allergic asthma in the United States and potential influence of future climate change. *Global Environmental and Occupational Health*, 1(3), 80–92. <https://doi.org/10.1002/2017GH000055>
- Ariya, P., Sun, J., Eltouny, N., Hudson, E. D., Hayes, C. T., & Kos, G. (2009). Physical and chemical characterization of bioaerosols—Implications for nucleation processes. *International Reviews in Physical Chemistry*, 28(1), 1–32. <https://doi.org/10.1080/01442350802597438>
- Arritt, R. W., Rink, T. D., Segal, M., Today, D. P., Clark, C. A., Mitchell, M. J., & Labas, K. M. (1997). The Great Plains low-level jet during the warm season of 1993. *Monthly Weather Review*, 125(9), 2176–2192. [https://doi.org/10.1175/1520-0493\(1997\)125<2176:TGPLLJ>2.0.CO;2](https://doi.org/10.1175/1520-0493(1997)125<2176:TGPLLJ>2.0.CO;2)
- Babin, S. M., Burkom, H. S., Holtry, R. S., Taberner, N. R., Stokes, L. D., Davies-Cole, J. O., et al. (2007). Pediatric patient asthma-related emergency department visits and admissions in Washington, DC, from 2001–2004, and associations with air quality, socio-economic status and age group. *Environmental Health*, 6(1), 9. <https://doi.org/10.1186/1476-069X-6-9>
- Bannister, T., Csutoros, D., Arnold, A. L., Black, J., Feren, G., Russell, R., et al. (2020). Are convergence lines associated with high asthma presentation days? A case-control study in Melbourne, Australia. *Science of the Total Environment*, 737, 140263. <https://doi.org/10.1016/j.scitotenv.2020.140263>
- Barth, M. C., Wong, J., Bela, M. M., Pickering, K. E., Li, Y., & Cummings, K. (2014). Simulations of lightning - Generated NO<sub>x</sub> for parameterized convection in the WRF - Chem model. In *Paper presented at 15th International Conference on Atmospheric Electricity, 15–20 June 2014, Norman, Oklahoma, U.S.A.*



- Bedka, K. M., & Mecikalski, J. R., (2005). Application of satellite-derived atmospheric vectors for estimating mesoscale flows. *Journal of Applied Meteorology*, 44(11), 1761–1772. <https://doi.org/10.1175/JAM2264.1>
- Beggs, P. J. (2017). Allergen aerosol from pollen-nucleated precipitation: A novel thunderstorm asthma trigger. *Atmospheric Environment*, 152, 455–457. <https://doi.org/10.1016/j.atmosenv.2016.12.045>
- Bellouin, N., Quaas, J., Gryspeerdt, E., Kinne, S., Stier, P., Watson-Parris, D., et al. (2020). Bounding global aerosol radiative forcing of climate change. *Reviews of Geophysics*, 58(1), e2019RG000660. <https://doi.org/10.1029/2019RG000660>
- Bigg, E. K. (1953). The formation of atmospheric ice crystals by the freezing of droplets. *Quarterly Journal of the Royal Meteorological Society*, 79(342), 510–519. <https://doi.org/10.1002/qj.49707934207>
- Brient, F., Schneider, T., Tan, Z., Bony, S., Qu, X., & Hall, A. (2015). Shallowness of tropical low clouds as a predictor of climate models response to warming. *Climate Dynamics*, 47(1), 433–449. <https://doi.org/10.1007/s00382-015-2846-0>
- Burkart, J., Gratzl, J., Seifried, T. M., Bieber, P., & Grothe, H. (2021). Subpollen particles (SPP) of birch as carriers of ice nucleating macromolecules. *Biogeosciences Discussions*, 1–15.
- Chen, F., & Dudhia, J. (2001). Coupling an advanced land surface-hydrology model with the Penn State-NCAR MM5 modeling system. Part I: Model implementation and sensitivity. *Monthly Weather Review*, 129(4), 569–585. [https://doi.org/10.1175/1520-0493\(2001\)129<0569:caalsh>2.0.co;2](https://doi.org/10.1175/1520-0493(2001)129<0569:caalsh>2.0.co;2)
- Chou, M., Suarez, M. J., Ho, C., Yan, M. M., & Lee, K. (1998). Parameterizations for cloud overlapping and shortwave single-scattering properties for use in general circulation and cloud ensemble models. *Journal of Climate*, 11(2), 202–214. [https://doi.org/10.1175/1520-0442\(1998\)011<0202:PF0COAS>2.0.CO;2](https://doi.org/10.1175/1520-0442(1998)011<0202:PF0COAS>2.0.CO;2)
- Christensen, M. W., Jones, W. K., & Stier, P. (2020). Aerosols enhance cloud lifetime and brightness along the stratus-to-cumulus transition. *Proceedings of the National Academy of Sciences of the United States of America*, 117(30), 17591–17598. <https://doi.org/10.1073/pnas.1921231117>
- Cooper, W. A. (1986). Ice initiation in natural clouds. *Meteorological Monographs*, 43, 29–32. <https://doi.org/10.1175/0065-9401-21.43.29>
- Dales, R. E., Cakmak, S., Judek, S., & Coates, F. (2008). Tree pollen and hospitalization for asthma in urban Canada. *International Archives of Allergy and Immunology*, 146(3), 241–247. <https://doi.org/10.1159/000116360>
- Dales, R. E., Cakmak, S., Judek, S., Dann, T., Coates, F., Brook, J. R., & Burnett, R. T. (2004). Influence of outdoor aeroallergens on hospitalization for asthma in Canada. *Journal of Allergy and Clinical Immunology*, 113(2), 303–306. <https://doi.org/10.1016/j.jaci.2003.11.016>
- D'Amato, G., Annesi-Maesano, I., Cecchi, L., & D'Amato, M. (2019). Latest news on relationship between thunderstorms and respiratory allergy, severe asthma, and deaths for asthma. *Allergy*, 74(1), 9–11. <https://doi.org/10.1111/all.13616>
- D'Amato, G., Vitale, C., D'Amato, M., Cecchi, L., Liccardi, G., Molino, A., et al. (2016). Thunderstorm-related asthma: What happens and why. *Clinical and Experimental Allergy*, 46(3), 390–396. <https://doi.org/10.1111/cea.12709>
- Darrow, L. A., Hess, J., Rogers, C. A., Tobert, P. E., Klein, M., & Sarnat, S. E. (2012). Ambient pollen concentrations and emergency department visits for asthma and wheeze. *Journal of Allergy and Clinical Immunology*, 130(3), 630–638.e4. <https://doi.org/10.1016/j.jaci.2012.06.020>
- Davis, M. B., & Brubaker, L. B. (1973). Differential sedimentation of pollen grains in lakes. *Limnology & Oceanography*, 18(4), 635–646. <https://doi.org/10.4319/lo.1973.18.4.0635>
- Dengate, H. N., Baruch, D. W., & Meredith, P. (1978). The density of wheat starch granules: A tracer dilution procedure for determining the density of an immiscible dispersed phase. *Starch*, 30(3), 80–84. <https://doi.org/10.1002/star.19780300304>
- Despres, V. R., Alex Huffman, J., Burrows, S. M., Hoose, C., Safatov, A. S., Buryak, G., et al. (2012). Primary biological aerosol particles in the atmosphere: A review. *Tellus Series B: Chemical and Physical Meteorology*, 64(1), 15598. <https://doi.org/10.3402/tellusb.v64i0.15598>
- Diehl, K., Quick, C., Matthias-Maser, S., Mitra, S. K., & Jaenicke, R. (2001). The ice nucleating ability of pollen: Part I: Laboratory studies in deposition and condensation freezing modes. *Atmospheric Research*, 58(2), 75–87. [https://doi.org/10.1016/S0169-8095\(01\)00091-6](https://doi.org/10.1016/S0169-8095(01)00091-6)
- Donovan, V. M., Wonkka, C. L., & Twidwell, D. (2017). Surging wildfire activity in a Grassland biome. *Geophysical Research Letters*, 44(12), 5986–5993. <https://doi.org/10.1002/2017GL072901>
- Dreischmeier, K., Budke, C., Wiehemeier, L., Kottke, T., & Koop, T. (2017). Boreal pollen contain ice-nucleating as well as ice-binding "anti-freeze" polysaccharides. *Scientific Reports*, 7, 1–13. <https://doi.org/10.1038/srep41890>
- Emmerson, K. M., Silver, J. D., Thatcher, M., Wain, A., Jones, P. J., Dowdy, A., et al. (2021). Atmospheric modelling of grass pollen rupture mechanisms for thunderstorm asthma prediction. *PLoS One*, 16(4), e0249488. <https://doi.org/10.1371/journal.pone.0249488>
- Emmons, L. K., Walters, S., Hess, P. G., Lamarque, J. F., Pfister, G. G., Fillmore, D., et al. (2010). Description and evaluation of the model for ozone and related chemical tracers, version 4 (MOZART-4). *Geoscientific Model Development*, 3(1), 43–67. <https://doi.org/10.5194/gmd-3-43-2010>
- Fan, J. W., Leung, L. R., Rosenfeld, D., Chen, Q., Li, Z. Q., Zhang, J. Q., & Yan, H. R. (2013). Microphysical effects determine macrophysical response for aerosol impacts on deep convective clouds. *Proceedings of the National Academy of Sciences of the United States of America*, 110(48), E4581–E4590. <https://doi.org/10.1073/pnas.1316830110>
- Fedorovich, E., Gibbs, J. A., & Shapiro, A. (2017). Numerical study of nocturnal low-level jets over gently sloping terrain. *Journal of the Atmospheric Sciences*, 74(9), 2813–2834. <https://doi.org/10.1175/JAS-D-17-0013.1>
- Fischer, H., Polikarpov, I., & Craievich, A. F. (2004). Average protein density is a molecular-weight-dependent function. *Protein Science*, 13(10), 2825–2828. <https://doi.org/10.1110/ps.04688204>
- Fröhlich-Nowoisky, J., Pickersgill, D. A., Despres, V. R., & Pöschl, U. (2009). High diversity of fungi in air particulate matter. *Proceedings of the National Academy of Sciences of the United States of America*, 106(31), 12814–12819. <https://doi.org/10.1073/pnas.0811003106>
- Grell, G. A., & Devenyi, D. (2002). A generalized approach to parameterizing convection combining ensemble and data assimilation techniques. *Geophysical Research Letters*, 29(4), 38–1–38-4. <https://doi.org/10.1029/2002GL015311>
- Grell, G. A., Peckham, S. E., Schmitz, R., McKeen, S. A., Wilczak, J., & Eder, B. (2005). Fully coupled "online" chemistry within the WRF model. *Atmospheric Environment*, 39(37), 6957–6975. <https://doi.org/10.1016/j.atmosenv.2005.04.027>
- Grote, M., Valenta, R., & Reichelt, R. (2003). Abortive pollen germination: A mechanism of allergen release in birch, alder, and hazel revealed by immunogold electron microscopy. *Journal of Allergy and Clinical Immunology*, 111(5), 1017–1023. <https://doi.org/10.1067/mai.2003.1452>
- Grote, M., Vrtala, S., Niederberger, V., Wiermann, R., Valenta, R., & Reichelt, R. (2001). Release of allergen-bearing cytoplasm from hydrated pollen: A mechanism common to a variety of grass (Poaceae) species revealed by electron microscopy. *Journal of Allergy and Clinical Immunology*, 108(1), 109–115. <https://doi.org/10.1067/mai.2001.116431>
- Guenther, A. B., Jiang, X., Heald, C. L., Sakulyanontvittaya, T., Duhl, T., Emmons, L. K., & Wang, X. (2012). The model of emissions of gases and aerosols from nature version 2.1 (MEGAN2.1): An extended and updated framework for modeling biogenic emissions. *Geoscientific Model Development*, 5(6), 1471–1492. <https://doi.org/10.5194/gmd-5-1471-2012>
- Gute, E., & Abbatt, J. P. D. (2018). Oxidative processing lowers the ice nucleation activity of birch and alder pollen. *Geophysical Research Letters*, 45(3), 1647–1653. <https://doi.org/10.1002/2017GL076357>

- Hallett, J., & Mossop, S. C. (1974). Production of secondary ice particles during the riming process. *Nature*, 249(5452), 26–28. <https://doi.org/10.1038/249026a0>
- Helbig, N., Vogel, B., Vogel, H., & Fiedler, F. (2004). Numerical modeling of pollen dispersion on the regional scale. *Aerobiologia*, 3(1), 3–19. <https://doi.org/10.1023/B:AERO.0000022984.51588.30>
- Hong, S. Y., Noh, Y., & Dudhia, J. (2006). A new vertical diffusion package with an explicit treatment of entrainment processes. *Monthly Weather Review*, 134(9), 2318–2341. <https://doi.org/10.1175/MWR3199.1>
- Hughes, D. D., Mampage, C. B. A., Jones, L. M., Liu, Z., & Stone, E. A. (2020). Characterization of atmospheric pollen fragments during spring-time thunderstorms. *Environmental Science and Technology Letters*, 7(6), 409–414. <https://doi.org/10.1021/acs.estlett.0c00213>
- Intergovernmental Panel on Climate Change (IPCC). (2021). In V. Masson-Delmotte, P. Zhai, A. Pirani, S. L. Connors, C. Péan, S. Berger, et al. (Eds.), *The Physical Science Basis. Contribution of Working Group I to the Sixth Assessment Report of the Intergovernmental Panel on Climate Change*. Cambridge University Press. <https://doi.org/10.1017/9781009157896>
- Jaenicke, R. (2005). Abundance of cellular material and proteins in the atmosphere. *Science*, 308(5718), 73. <https://doi.org/10.1126/science.1106335>
- Janjic, Z. I. (2002). Nonsingular implementation of the Mellor–Yamada level 2.5 scheme in the NCEP Meso model. *NCEP Office Note*, 437, 61.
- Jones, A. M., & Harrison, R. M. (2004). The effects of meteorological factors on atmospheric bioaerosol concentrations. *Science of the Total Environment*, 326(1–3), 151–180. <https://doi.org/10.1016/j.scitotenv.2003.11.021>
- Joung, Y. S., Ge, Z., & Buie, C. R. (2017). Bioaerosol generation by raindrops on soil. *Nature Communications*, 8(1), 14668. <https://doi.org/10.1038/ncomms14668>
- Kawecki, S., & Steiner, A. L. (2018). The influence of aerosol hygroscopicity on precipitation intensity during a mesoscale convective event. *Journal of Geophysical Research: Atmospheres*, 123(1), 424–442. <https://doi.org/10.1002/2017JD026535>
- Kevat, A. (2020). Thunderstorm asthma: Looking back and looking forward. *Journal of Asthma and Allergy*, 13, 293–299. <https://doi.org/10.2147/jaa.s265697>
- Knopf, D. A., Barry, K. R., Brubaker, T. A., Jahl, L. G., Jankowski, K. L., Li, J., et al. (2021). Aerosol–ice formation closure: A Southern Great Plains field campaign. *Bulletin of the American Meteorological Society*, 102(10), E1952–E1971. <https://doi.org/10.1175/BAMS-D-20-0151.1>
- Kuparinen, A., Katul, G., Nathan, R., & Schurr, F. M. (2009). Increases in air temperature can promote wind-driven dispersal and spread of plants. *Proceedings of the Royal Society of London B*, 276(1670), 3081–3087. <https://doi.org/10.1098/rspb.2009.0693>
- Kuparinen, A., Markkanen, T., Riikonen, H., & Vesala, T. (2007). Modeling air-mediated dispersal of spores, pollen and seeds in forested areas. *Ecological Modelling*, 208(2–4), 177–188. <https://doi.org/10.1016/j.ecolmodel.2007.05.023>
- Kuparinen, A., Schurr, F., Tackenberg, O., & O'Hara, R. B. (2007). Air mediated pollen flow from genetically modified to conventional crops. *Ecological Applications*, 17(2), 431–440. <https://doi.org/10.1890/05-1599>
- Lake, I. R., Jones, N. R., Agnew, M., Goodess, C. M., Giorgi, F., Hamaoui-Laguel, L., et al. (2016). Climate change and future pollen allergy in Europe. *Environmental Health Perspectives*, 125(3), 385–391. <https://doi.org/10.1289/EHP173>
- Lawler, M. J., Draper, D. C., & Smith, J. N. (2020). Atmospheric fungal nanoparticle bursts. *Science Advances*, 6(3). <https://doi.org/10.1126/sciadv.aax9051>
- Lewis, W. H., Vinay, P., & Zenger, V. E. (1983). *Airborne and allergenic pollen of North America*. The John Hopkins University Press.
- Linkosalo, T., Ranta, H., Oksanen, A., Siljamo, P., Luomajoki, A., Kukkonen, J., & Sofiev, M. (2010). A double-threshold temperature sum model for predicting the flowering duration and relative intensity of *Betula pendula* and *B. pubescens*. *Agricultural and Forest Meteorology*, 150(12), 6–11. <https://doi.org/10.1016/j.agrformet.2010.08.007>
- Maddox, R. A. (1983). Large-scale meteorological conditions associated with midlatitude mesoscale convective complexes. *Monthly Weather Review*, 111(7), 1475–1493. [https://doi.org/10.1175/1520-0493\(1983\)111<1475:LSMCAW>2.0.CO;2](https://doi.org/10.1175/1520-0493(1983)111<1475:LSMCAW>2.0.CO;2)
- Mahura, A., Korsholm, U., Baklanov, A., & Rasmussen, A. (2007). Elevated birch pollen episodes in Denmark: Contributions from remote sources. *Aerobiologia*, 23(3), 171–179. <https://doi.org/10.1007/s10453-007-9061-3>
- Malm, W. C., Sisler, J. F., Huffman, D., Eldred, R. A., & Cahill, T. A. (1994). Spatial and seasonal trends in particle concentration and optical extinction in the United States. *Journal of Geophysical Research*, 99(D1), 1347–1370. <https://doi.org/10.1029/93JD02916>
- Marousis, S. N., & Saravacos, G. D. (1990). Density and porosity in drying starch materials. *Journal of Food Science*, 55(5), 1367–1372. <https://doi.org/10.1111/j.1365-2621.1990>
- Maupin, C. R., Roark, E. B., Thirumalai, K., Shen, C. C., Schumacher, C., Kampen-Lewis, S. V., et al. (2021). Abrupt Southern Great Plains thunderstorm shifts linked to glacial climate variability. *Nature Geoscience*, 14(6), 396–401. <https://doi.org/10.1038/s41561-021-00729-w>
- Melvin, M. (2018). *National prescribed fire use survey report Technical Report 03-18 Coalition of Prescribed Fire Councils*. Inc National Strategy.
- Meyers, M. P., DeMott, P. J., & Cotton, W. R. (1992). New primary ice-nucleation 924 parameterizations in an explicit cloud model. *Journal of Applied Meteorology*, 31(7), 708–721. [https://doi.org/10.1175/1520-0450\(1992\)0312.0.CO;2](https://doi.org/10.1175/1520-0450(1992)0312.0.CO;2)
- Miguel, A. G., Taylor, P. E., House, J., Glover, M. M., & Flagan, R. C. (2006). Meteorological influences on respirable fragment release from Chinese elm pollen. *Aerosol Science and Technology*, 40(9), 690–696. <https://doi.org/10.1080/02786820600798869>
- Mlawer, E. J., Taubman, S. J., Brown, P. D., Iacono, M., & Clough, S. A. (1997). Radiative transfer for inhomogeneous atmospheres: RRTM, a validated correlated-k model for the longwave. *Journal of Geophysical Research*, 102(D14), 16663–16682. <https://doi.org/10.1029/97JD00237>
- Mo, K. C., & Berbery, E. H. (2004). Low-level jets and the summer precipitation regimes over North America. *Journal of Geophysical Research*, 109(D6), 006117. <https://doi.org/10.1029/2003JD004106>
- Monin, A. S., & Obukhov, A. M. (1954). Basic laws of turbulent mixing in the surface layer of the atmosphere. *Contributions of the Geophysical Institute of the Slovak Academy of Science, USSR*, 151, 163–187.
- Morrison, H., Curry, J. A., & Khvorostyanov, V. I. (2005). A new double-moment microphysics parameterization for application in cloud and climate models. Part I: Description. *Journal of the Atmospheric Sciences*, 62(6), 1665–1677. <https://doi.org/10.1175/jas3446.1>
- Murray, B. J., O'Sullivan, D., Atkinson, J. D., & Webb, M. E. (2012). Ice nucleation by particles immersed in supercooled cloud droplets. *Chemical Society Reviews*, 41(19), 6519–6554. <https://doi.org/10.1039/C2CS35200A>
- Nathan, R., Horvitz, N., He, Y., Kuparinen, A., Schurr, F. M., & Katul, G. G. (2011). Spread of North-American wind-dispersed trees in future environments. *Ecology Letters*, 14(3), 211–219. <https://doi.org/10.1111/j.1461-0248.2010.01573.x>
- Neumann, J. E., Anenberg, S. C., Weinberger, K. R., Amend, M., Gulati, S., Crimmins, A., et al. (2019). Estimates of present and future asthma emergency department visits associated with exposure to oak, birch, and grass pollen in the United States. *Global Environmental and Occupational Health*, 3(1), 11–27. <https://doi.org/10.1029/2018GH000153>
- Newson, R., Strachan, D., Archibald, E., Emberlin, J., Hardaker, P., & Collier, C. (1998). Acute asthma epidemics, weather and pollen in England, 1987–1994. *European Respiratory Journal*, 11(3), 694–701. <https://doi.org/10.1136/THX.52.8.680>
- NIFC. (2019). National Interagency Fire Center. Retrieved from [https://www.nifc.gov/fireInfo/fireInfo\\_stats\\_lgFires.html](https://www.nifc.gov/fireInfo/fireInfo_stats_lgFires.html)



- Parworth, C., Fast, J., Mei, F., Shippert, T., Sivaraman, C., Tilp, A., et al. (2015). Long-term 655 measurements of submicrometer aerosol chemistry at the Southern Great Plains (SGP) using an Aerosol Chemical Speciation Monitor (ACSM). *Atmospheric Environment*, *106*, 43–55. <https://doi.org/10.1016/j.atmosenv.2015.01.060>
- Penner, J. E., Dong, X. Q., & Chen, Y. (2004). Observational evidence of a change in radiative forcing due to the indirect aerosol effect. *Nature*, *427*(6971), 231–234. <https://doi.org/10.1038/nature02234>
- Pollock, J., Lu, S., & Gimbel, R. W. (2017). Outdoor environment and pediatric asthma: An update on the evidence from North America. *Canadian Respiratory Journal*, *2017*, 1–16. <https://doi.org/10.1155/2017/8921917>
- Pöschl, U., Martin, S. T., Sinha, B., Chen, Q., Gunthe, S. S., Huffman, J. A., et al. (2010). Rainforest aerosols as biogenic nuclei of clouds and precipitation in the Amazon. *Science*, *329*(5998), 1513–1516. <https://doi.org/10.1126/science.1191056>
- Posselt, R., & Lohmann, U. (2008). Influence of Giant CCN on warm rain processes in the ECHAM5 GCM. *Atmospheric Chemistry and Physics*, *8*(14), 3769–3788. <https://doi.org/10.5194/acp-8-3769-2008>
- Pummer, B. G., Bauer, H., Bernardi, J., Bleicher, S., & Grothe, H. (2012). Suspendable macromolecules are responsible for ice nucleation activity of birch and conifer pollen. *Atmospheric Chemistry and Physics*, *12*(5), 2541–2550. <https://doi.org/10.5194/acp-12-2541-2012>
- Rathnayake, C. M., Metwali, N., Jayarathne, T., Kettler, J., Huang, Y., Thorne, P. S., et al. (2017). Influence of rain on the abundance of bioaerosols in fine and coarse particles. *Atmospheric Chemistry and Physics*, *17*(3), 2459–2475. <https://doi.org/10.5194/acp-17-2459-2017>
- Schell, B., Ackerman, I. J., Hass, H., Binkowski, F. S., & Ebel, A. (2001). Modelling the formation of secondary organic aerosol within a comprehensive air quality model system. *Journal of Geophysical Research*, *106*(D22), 28275–28293. <https://doi.org/10.1029/2001JD000384>
- Sofiev, M., Siljamo, P., Ranta, H., Linkosalo, T., Jaeger, S., Rasmussen, A., et al. (2013). A numerical model of birch pollen emission and dispersion in the atmosphere. Description of the emission module. *International Journal of Biometeorology*, *57*(1), 45–58. <https://doi.org/10.1007/s00484-012-0532-z>
- Sofiev, M., Siljamo, P., Ranta, H., & Rantio-Lehtimäki, A. (2006). Towards numerical forecasting of long-range air transport of birch pollen: Theoretical considerations and a feasibility study. *International Journal of Biometeorology*, *50*(392), 392–402. <https://doi.org/10.1007/s00484-006-0027-x>
- Steiner, A. L., Brooks, S. D., Deng, C., Thornton, D. C. O., Pendleton, M. W., & Bryant, V. (2015). Pollen as atmospheric cloud condensation nuclei. *Geophysical Research Letters*, *42*(9), 3596–3602. <https://doi.org/10.1002/2015GL064060>
- Steiner, J. L., Wetter, J., Robertson, S., Teet, S., Wang, J., Wu, X., et al. (2020). Grassland wildfires in the Southern Great Plains: Monitoring ecological impacts and recovery. *Remote Sensing*, *12*(619), 619. <https://doi.org/10.3390/rs1204061>
- Stockwell, W. R., Middleton, P., Chang, J. S., & Tang, X. (1990). The second generation regional acid deposition model chemical mechanism for regional air quality modeling. *Journal of Geophysical Research*, *95*(D10), 16343–16367. <https://doi.org/10.1029/JD095iD10p16343>
- Stone, E. A., Mampage, C. B. A., Hughes, D. D., & Jones, L. M. (2021). Airborne sub-pollen particles from rupturing giant ragweed pollen. *Aerobiologia*, *37*(3), 625–632. <https://doi.org/10.1007/s10453-021-09702-x>
- Straka, H. (1975). *Pollen-und Sporenkunde. Grundbegriffe der modernen Biologie 13*. Gustav Fischer.
- Subba, T., Lawler, M. J., & Steiner, A. L. (2021). Estimation of possible primary biological particle emissions and rupture events at the Southern Great Plains ARM site. *Journal of Geophysical Research: Atmospheres*, *126*(16), e2021JD034679. <https://doi.org/10.1029/2021JD034679>
- Sun, J., & Ariya, P. (2006). Atmospheric organic and bio-aerosols as cloud condensation nuclei (CCN): A review. *Atmospheric Environment*, *40*(5), 795–820. <https://doi.org/10.1016/j.atmosenv.2005.05.052>
- Suphioglu, C., Singh, M. B., Taylor, P., Knox, R. B., Bellomo, R., Holmes, P., & Puy, R. (1992). Mechanism of grass-pollen-induced asthma. *The Lancet*, *339*(8793), 569–572. [https://doi.org/10.1016/0140-6736\(92\)90864-Y](https://doi.org/10.1016/0140-6736(92)90864-Y)
- Tackenberg, O. (2003). Modeling long distance dispersal of plant diaspores by wind. *Ecological Monographs*, *73*(2), 173–189. [https://doi.org/10.1890/0012-9615\(2003\)073\[0173:MLDOPD\]2.0.CO;2](https://doi.org/10.1890/0012-9615(2003)073[0173:MLDOPD]2.0.CO;2)
- Tang, M., Gu, W., Ma, Q., Li, Y. J., Zhong, C., Li, S., et al. (2019). Water adsorption and hygroscopic growth of six anemophilous pollen species: The effect of temperature. *Atmospheric Chemistry and Physics*, *19*(4), 2247–2258. <https://doi.org/10.5194/acp-19-2247-2019>
- Taylor, P. E., Flagan, R. C., Miguel, A. G., Valenta, R., & Glovsky, M. M. (2004). Birch pollen rupture and the release of aerosols of respirable allergens. *Clinical and Experimental Allergy*, *34*(10), 1591–1596. <https://doi.org/10.1111/j.1365-2222.2004.02078>
- Taylor, P. E., Flagan, R. C., Valenta, R., & Glovsky, M. M. (2002). Release of allergens as respirable aerosols: A link between grass pollen and asthma. *Journal of Allergy and Clinical Immunology*, *109*(1), 51–56. <https://doi.org/10.1067/mai.2002.120759>
- Taylor, P. E., & Jonsson, H. (2004). Thunderstorm asthma. *Current Allergy and Asthma Reports*, *4*(5), 409–413. <https://doi.org/10.1007/s11882-004-0092-3>
- Thien, F., Beggs, P. J., Csutoros, D., Darvall, J., Hew, M., Davies, J. M., et al. (2018). The Melbourne epidemic thunderstorm asthma event 2016: An investigation of environmental triggers, effect on health services, and patient risk factors. *The Lancet Planetary Health*, *2*(2), 255–263. [https://doi.org/10.1016/S2542-5196\(18\)30120-7](https://doi.org/10.1016/S2542-5196(18)30120-7)
- Veriankaitė, L., Siljamo, P., Sofiev, M., Šaulienė, I., & Kukkonen, J. (2010). Modeling analysis of source regions of long-range transported birch pollen that influences allergenic seasons in Lithuania. *Aerobiologia*, *26*(1), 47–62. <https://doi.org/10.1007/s10453-009-9142-6>
- Vial, J., Bony, S., Dufresne, J. L., & Roeckig, R. (2016). Coupling between lower-tropospheric convective mixing and low-level clouds: Physical mechanisms and dependence on convection scheme. *Journal of Advances in Modeling Earth Systems*, *8*(4), 1892–1911. <https://doi.org/10.1002/2016MS000740>
- Vial, J., Bony, S., Stevens, B., & Vogel, R. (2017). Mechanisms and model diversity of trade-wind shallow cumulus cloud feedbacks: A review. *Surveys in Geophysics*, *38*(6), 1331–1353. <https://doi.org/10.1007/s10712-017-9418-2>
- Wozniak, M. C., Solmon, F., & Steiner, A. L. (2018). Pollen rupture and its impact on precipitation in clean continental conditions. *Geophysical Research Letters*, *45*(14), 7156–7164. <https://doi.org/10.1029/2018GL077692>
- Wozniak, M. C., & Steiner, A. L. (2017). A prognostic pollen emissions model for climate models (PECM1.0). *Geoscientific Model Development*, *10*(11), 1–36. <https://doi.org/10.5194/gmd-10-4105-2017>
- Yair, Y., Yair, Y., Rubin, B., Confino-Cohen, R., Rosman, Y., Shachar, E., & Rottem, M. (2019). First reported case of thunderstorm asthma in Israel. *Natural Hazards Earth System Science*, *19*(12), 2715–2725. <https://doi.org/10.5194/nhess-19-2715-2019>
- Yin, Y., Levin, Z., Reisin, T. G., & Tzivion, S. (2000). The effects of giant cloud condensation nuclei on the development of precipitation in convective clouds – A numerical study. *Atmospheric Research*, *53*(1–3), 91–116. [https://doi.org/10.1016/s0169-8095\(99\)00046-0](https://doi.org/10.1016/s0169-8095(99)00046-0)
- Zhang, R., Duhl, T., Salam, M. T., House, J. M., Flagan, R. C., Avol, E. L., et al. (2014). Development of a regional-scale pollen emission and transport modeling framework for investigating the impact of climate change on allergic airway disease. *Biogeosciences*, *11*(6), 1461–1478. <https://doi.org/10.5194/bg-11-1461-2014>
- Zhang, Y., Bielory, L., & Georgopoulos, P. (2014). Climate change effect on *Betula* (birch) and *Quercus* (oak) pollen seasons in US. *International Journal of Biometeorology*, *58*(5), 909–919. <https://doi.org/10.1007/s00484-013-0674-7>

- Zhang, Y., & Steiner, A. L. (2022). Projected climate-driven changes in pollen emission season length and magnitude over the continental United States. *Nature Communications*, *13*(1), 1234. <https://doi.org/10.1038/s41467-022-28764-0>
- Zhu, Q., Laughner, J. L., & Cohen, R. C. (2019). Lightning NO<sub>2</sub> simulation over the contiguous US and its effects on satellite NO<sub>2</sub> retrievals. *Atmospheric Chemistry and Physics*, *19*(20), 13067–13078. <https://doi.org/10.5194/acp-19-13067-2019>
- Ziska, L., Knowlton, K., Rogers, C., Dalan, D., Tierney, N., Elder, M. A., et al. (2011). Recent warming by latitude associated with increased length of ragweed pollen season in central North America. *Proceedings of the National Academy of Sciences, USA*, *108*(10), 4248–4251. <https://doi.org/10.1073/pnas.1014107108>